Molecular Medicine

RESEARCH ARTICLE

Open Access

Skeletal myotubes expressing ALS mutant SOD1 induce pathogenic changes, impair mitochondrial axonal transport, and trigger motoneuron death

Pablo Martínez[1], Mónica Silva[2], Sebastián Abarzúa[1], María Florencia Tevy[3], Enrique Jaimovich[2], Martha Constantine-Paton[4], Fernando J. Bustos[1,5*] and Brigitte van Zundert[1,5,6*]

Abstract

Amyotrophic lateral sclerosis (ALS) is a fatal neurodegenerative disease characterized by the loss of motoneurons (MNs), and despite progress, there is no effective treatment. A large body of evidence shows that astrocytes expressing ALS-linked mutant proteins cause non-cell autonomous toxicity of MNs. Although MNs innervate muscle fibers and ALS is characterized by the early disruption of the neuromuscular junction (NMJ) and axon degeneration, there are controversies about whether muscle contributes to non-cell-autonomous toxicity to MNs. In this study, we generated primary skeletal myotubes from myoblasts derived from ALS mice expressing human mutant SOD1^{G93A} (termed hereafter mutSOD1). Characterization revealed that mutSOD1 skeletal myotubes display intrinsic phenotypic and functional differences compared to control myotubes generated from non-transgenic (NTg) littermates. Next, we analyzed whether ALS myotubes exert non-cell-autonomous toxicity to MNs. We report that conditioned media from mutSOD1 myotubes (mutSOD1-MCM), but not from control myotubes (NTg-MCM), induced robust death of primary MNs in mixed spinal cord cultures and compartmentalized microfluidic chambers. Our study further revealed that applying mutSOD1-MCM to the MN axonal side in microfluidic devices rapidly reduces mitochondrial axonal transport while increasing Ca2 + transients and reactive oxygen species (i.e., H_2O_2). These results indicate that soluble factor(s) released by mutSOD1 myotubes cause MN axonopathy that leads to lethal pathogenic changes.

Keywords ALS, Myotubes, Muscle, Motoneuron, Axonopathy, Mitochondria, Pathology

*Correspondence:
Fernando J. Bustos
fernando.bustos@unab.cl
Brigitte van Zundert
bvanzundert@unab.cl
[1] Institute of Biomedical Sciences (ICB), Faculty of Medicine & Faculty of Life Sciences, Universidad Andres Bello, Santiago, Chile
[2] Center for Exercise, Metabolism and Cancer, Facultad de Medicina, Instituto de Ciencias Biomédicas, Universidad de Chile, Santiago, Chile
[3] Facultad de Medicina, Universidad de Atacama, Copiapó, Chile
[4] McGovern Institute for Brain Research, Department of Brain and Cognitive Sciences, Massachusetts Institute of Technology, Cambridge, MA, USA
[5] Millennium Nucleus of Neuroepigenetics and Plasticity (EpiNeuro), Santiago, Chile
[6] Department of Neurology, University of Massachusetts Chan Medical School (UMMS), Worcester, MA, USA

Introduction

Amyotrophic lateral sclerosis (ALS) is a progressive and fatal neurodegenerative disease characterized by the loss of upper and lower motoneurons (MNs), muscle wasting, and paralysis (Al-Chalabi and Hardiman 2013; Peters et al. 2015; Taylor et al. 2016). Some cases of ALS arise in association with frontotemporal dementia (FTD) (Ling et al. 2013). Sporadic ALS (sALS) cases are responsible for most of the cases (90%), while the remaining 10% have a familial history of ALS (fALS), characterized by genetic inheritance (Renton et al. 2014). Approximately 20% of fALS corresponds to mutations in the superoxide dismutase 1 (mutSOD1) gene, where more than 160 mutations have now been identified in its sequence (http://alsod.iop.kcl.ac.uk/). The discovery of SOD1 mutations in fALS patients (Rosen et al. 1993) led to the generation of the first transgenic ALS mouse model expressing $SOD1^{G93A}$ (Gurney et al. 1994). As of today, the high copy number $SOD1^{G93A}$ transgenic mouse model is still a cornerstone of ALS research because this model closely recapitulates the human clinical and histopathological symptoms of ALS and exhibits a stable and well-established disease progression, enabling preclinical testing of novel genes and pharmacological therapies (Zundert and Brown 2017).

Based on studies in vitro with cultures and in vivo with mouse models, it is widely accepted that MN degeneration in ALS occurs through non-cell-autonomous mechanisms, involving interactions between various local cell types such as astrocytes, microglia, and oligodendrocytes (Ilieva et al. 2009; Maimon and Perlson 2019). Particularly, there is compelling evidence that ALS astrocytes cause non-cell-autonomous toxicity to MNs (Harten et al. 2021; Dittlau and Bosch 2023; Garcés et al. 2024). For example, in in vivo studies, the survival of mutSOD1 mice is significantly extended when ALS MNs are surrounded by wild-type (WT) non-neuronal cells (Clement et al. 2003), particularly astrocytes (Lepore et al. 2008). Selective deletion of the mutSOD1 genes from astrocytes markedly prolongs the survival of the mutSOD1 mice by delaying disease onset and/or progression (Yamanaka et al. 2008; Wang et al. 2011). Conversely, studies in rodents, either by selectively expressing ALS-linked mutant genes or by transplanting glial progenitors, suggest that fALS astrocytes (Papadeas et al. 2011; Tong et al. 2013), and sALS astrocytes (Qian et al. 2017) can induce certain aspects of MN degeneration, locomotor deficits, and decrease survival. Non-cell autonomous toxicity to MNs induced by cultured astrocytes harboring diverse ALS-causing gene mutations, including mutations in SOD1, TDP43, and C9ORF72, has also been extensively documented (Harten et al. 2021; Dittlau and Bosch 2023; Garcés et al. 2024). Our recent study further reveals that excessive inorganic polyphosphate (polyP) released by ALS astrocytes triggers MN death and increases neuronal excitability and Ca^{2+} transients (Arredondo et al. 2022; Rojas et al. 2023; Garcés et al. 2024). Additionally, other studies have also shown that astrocyte-mediated MN degeneration is accompanied by several other pathogenic events, including oxidative stress, induction of a cell death signaling (i.e., phosphorylation of c-Abl), and impaired mitochondrial transport (Haidet-Phillips et al. 2011; Fritz et al. 2013; Rojas et al. 2014, 2015; Birger et al. 2019; Harten et al. 2021; Dittlau and Bosch 2023).

In addition to astrocytes, studies in patients and animal models indicate that cells outside the central nervous system (CNS) are also affected in ALS, including lymphocytes (Cova et al. 2006), fibroblasts (Aguirre et al. 1998), and skeletal muscle (Frey et al. 2000; Hegedus et al. 2007; Dobrowolny et al. 2008; Wong and Martin 2010; Jensen et al. 2016; Cappello and Francolini 2017; Guo et al. 2020a). Regarding the latter, while MNs innervate muscle fibers and ALS is characterized by the early disruption of the neuromuscular junction (NMJ) and axon degeneration (Fischer et al. 2004; Moloney et al. 2014; Cappello and Francolini 2017; Guo et al. 2020a), there are controversies whether muscle contributes to MN degeneration. While reducing SOD1 levels directly in the muscles of mutSOD1 transgenic mice did not affect the onset of the disease or survival (Miller et al. 2006) muscle-restricted expression of mutSOD1 led to alterations associated with ALS pathogenesis (Dobrowolny et al. 2009) and a classic ALS mouse phenotype (Dobrowolny et al. 2009; Wong and Martin 2010; Maimon et al. 2018). Studies with cultures also report controversial results. Recent data favoring the contribution of non-cell autonomous toxicity of muscle-secreted factors on ALS demonstrated that myocytes express and release Sema3A that leads to NMJ disruption and axon degeneration (Maimon et al. 2018). Another recent study showed an altered secreted metabolome of mutSOD1 myocytes (Stella et al. 2023). Conversely, previous evidence did not show any effect on MN survival when treated with media conditioned by myocytes expressing mutSOD1 (Nagai et al. 2007).

Here, we demonstrate that myotube-conditioned media (MCM) derived from primary myotubes harboring mutated human $SOD1^{G93A}$ (mutSOD1-MCM) induce MN death and trigger the accumulation of ROS and phosphorylated c-Abl. Furthermore, we found that distal application of mutSOD1-MCM increases intracellular Ca^{2+} events, ROS production, and death of primary wild-type MNs using microfluidic devices. We also found that MCM-mutSOD1 produces a functional deficit of axonal mitochondrial transport, both retrograde and anterograde. Our findings provide compelling evidence

that myotubes contribute to MN degeneration in SOD1-linked ALS.

Materials and methods

Mice handling

All mice used were handled according to the guidelines for the handling and care of experimentation established by the NIH (NIH, Maryland, USA) and following the protocol approved by the bioethics committee of Andres Bello University (approval certificate 014/2017). We used hemizygous transgenics mice harboring the human mutation $SOD1^{G93A}$ (High number of copies; B6SJL) obtained from Laboratories Jackson (Cat. No. 0022726, Bar Harbor, ME, USA). Non-transgenic littermates were used as controls. The presence of the transgene was identified by end-point PCR (Fritz et al. 2013).

Myoblasts and myotubes cultures

Cultures of myoblasts and myotubes were made from postnatal days 1–4 (P1-4) pups as described previously (Valdés et al. 2007). Briefly, pups were euthanized by decapitation and left in PBS 1X (Hyclone, No.SH30538.03). Muscle tissue was obtained from lower limbs and incubated for 15 min at 37℃ in a collagenase type-2 (1.5 mg/mL; Gibco, No.17101–015), dissolved in PBS 1X and filtered with 0.22 µm filters. Then, the tissue was mechanically disintegrated and incubated for 15 min at 37℃ with the collagenase solution. Subsequently, it was mechanically disintegrated for a second time and 5 ml of F-10 medium was added (Sigma, No. 6635-1L). The solution was filtered through 40 µm filters (Falcon, No. 352340) and centrifuged at 1100 RPM for 7 min. The supernatant was removed and the pellet was resuspended in myoblast growing media F-10 supplemented with 20% bovine growth serum (BGS, Hyclone, No. SH30541.03), 1% penicillin/streptomycin (Gibco, No. 15114-122), and five ng/mL final concentration of human fibroblast growth factor (FGF; PeproTech, No. 100-18B-100UG). Cells were plated in 100 mm plates (without any matrix) for 45 min at 37 ℃ and 5% CO2. After this time, adhered fibroblasts were observed and the supernatant containing the myoblasts was removed and plated on a new 100 mm plate treated with Matrigel (Sigma, No. E1270). The culture medium was replaced every two days. When myoblasts reached 70% confluency (3–5 DIV), growing media was replaced by differentiation media that consisted of DMEM (Gibco, No. 11885-084) supplemented with 10% fetal bovine serum (FBS; Gibco, No. 16000-044), 4% horse serum (Gibco, No. 16050), 1% L-glutamine (Gibco, No. 25030) and 1% penicillin/streptomycin. The fusion of myoblasts was observed from the second day after the medium change. The differentiation medium was replaced every four days until the complete fusion and differentiation to myotubes (~ 10 DIV after medium change), which showed spontaneous contractions under the light microscope.

Spontaneous contraction assay

Myotube cultures were visualized using an epifluorescence microscope (Nikon Eclipse Ti-U; objective 20X) 10 DIV after differentiation. Spontaneous contractions were observed and quantified manually and normalized to 1 min.

Preparation of myotube-conditioned media

Conditioned media was prepared from primary cultures of myotubes. At 80–90% of confluence (8–10 DIV after differentiation induction) culture medium was replaced by ventral spinal cord neurons growth media (Fritz et al. 2013), containing 70% MEM (Life technologies 11,090–073), 25% Neurobasal media (Life technologies 21,103–049), 1% N2 supplement (Life technologies 17,502–048), 1% L-glutamine (Life technologies 25,030–081), 1% penicillin–streptomycin (Life technologies 15,070–063), 2% horse serum (Hyclone SH30074.03) and 1 mM pyruvate (Sigma). The media was left for seven days, supplemented with D(+)Glucose (Sigma, No.G7021), and filtered with 0.22 µm filters. The myotube conditioning media (MCM) was stored at -80℃ for six months.

Primary ventral spinal cord cultures

Sprague Dawley rats were cared for and handled according to the guideline practices of managing and caring for experimental animals established by the NIH (NIH, Maryland, USA) and following the approval of the Ethics Committee of Andres Bello University. Primary ventral spinal cord cultures were prepared from embryonic day 18 (E18) rats as previously described by our laboratory (Sepulveda et al. 2010; Fritz et al. 2013). Briefly, pregnant wild-type rats were euthanized using a CO2 chamber, and E18 embryos were removed and rapidly decapitated. Tissues were placed in a cold PBS 1X solution supplemented with 1% penicillin/streptomycin. The dorsal portion of the cord was removed using a sterile scalpel. The ventral spinal cords were mechanically dissociated and incubated for 20 min at 37℃ in prewarmed 1X PBS supplemented with 0.25% trypsin (Life Technologies 15,090–046). After incubation, cells were transferred to 15 ml tubes containing feeding medium: Minimum Essential Media (MEM; Life Technologies, 11,095–072) supplemented with 10% Horse serum (Hyclone, SH30074.03), 1% L-glutamine (Life Technologies, 25,030–081), 4 mg/mL DNAase (Roche, 04716728001). Cells were resuspended by mechanical agitation through Pasteur pipettes flamed with decreasing diameters. Cells were counted and seeded (400,000 cells/mL for survival assays) on

poly-L-lysine treated glasses (MW 350 kDa, Sigma Chemical, St. Louis, MO). Feeding medium was replaced for growth media: 70% MEM (Life technologies 11,090–073), 25% Neurobasal media (Life technologies 21,103–049), 1% N2 supplement (Life technologies 17,502–048), 1% L-glutamine (Life technologies 25,030–081), 1% penicillin–streptomycin (Life technologies 15,070–063), 2% horse serum (Hyclone SH30074.03) and 1 mM pyruvate (Sigma S8636). Cultures were supplemented with 45 µg/ml of E18 chicken leg extract kept at 37 ℃ and 5% CO2, with medium replaced every 3 days.

Immunofluorescence

For myoblast and myotube cultures characterization, MN survival, and c-Abl phosphorylation, immunofluorescence assays were performed on 4% PFA (20 min) fixed cultures, followed by three washes with PBS 1X. Then, cells were permeabilized with Triton X-100 at 0.05% v/v in PBS 1X for 30 min and washed three times with PBS 1X. Cells were blocked for 30 min with goat serum (Life Technologies, No. 50062Z). Cells were incubated with the different primary antibodies overnight at 4℃. Primary antibodies used were: Pax7 (DSHB, AB_528428, 1:100), SMI32 (Abcam, Ab187374, 1:500), MAP2 (Merck Millipore, Mab378, 1:250), MyoD (DSHB, D7F2-s, 1:500), MHC (Novus Biologicals, NB300-284, 1:1000), Myogenin (Abcam, Ab1835, 1:500) and c-Abl Tyr-412 (SIGMA, C5240, 1:1000). The next day, cells were washed three times with PBS 1X for 5 min each wash and incubated with the secondary antibodies conjugated to Alexa 488, Alexa 555, or Alexa 633 for 2.5 h at room temperature. Secondary antibodies used: goat anti-rabbit Alexa Fluor 488 (Life Technologies, A11008, 1:500), goat anti-mouse Alexa Fluor 488 (Life Technologies, A10667, 1:500), goat anti-rabbit Alexa Fluor 555 (Life Technologies, A21428, 1:500), goat anti-mouse Alexa Fluor 555 (Life Technologies, A21422, 1:500), goat anti-rabbit Alexa Fluor 633 (Life Technologies, A21070, 1:500), goat anti-mouse Alexa Fluor 633 (Life Technologies, A21050, 1:500). In parallel to the secondary antibodies' incubation, cells were incubated with DAPI (Sigma, No. D9542). Cells were then washed three times for 5 min in PBS 1X and mounted using Fluoromont G fluorescence mounting medium (EMS, No. 17984–25). For all immunofluorescence analysis, we used an epifluorescence microscope (Nikon Eclipse Ti-U; objective 20X).

MN survival assay

Survival of MNs was measured as previously described by our laboratory (Fritz et al. 2013; Rojas et al. 2014). Briefly, spinal cord cultures were fixed at 7 DIV, and immunofluorescence was performed using the above protocol. We used a specific antibody for MAP2 to detect all neurons in the cultures (including interneurons and MNs) and a specific antibody for SMI32 to identify only MNs (Nagai et al. 2007; Sepulveda et al. 2010; Fritz et al. 2013; Mishra et al. 2020; Arredondo et al. 2022). Previously, we have described that primary spinal cord cultures contain 8–10% of MNs at 12 DIV (Sepulveda et al. 2010). Fluorescent staining was visualized by epifluorescence microscopy (Nikon Eclipse Ti-U; objective 20X). The fields with neurons were randomly chosen, and the number of MAP2 + and SMI32 + neurons was counted from all the acquired images. Per condition, ≥ ten randomly selected fields (≥ 200 cells) were analyzed to calculate the percentage of SMI32 + MNs for the total number of MAP2 + cells. The ratio between $SMI32^+/MAP2^+$-cells and $SMI32^-/MAP2^+$ neurons indicate the percentage of MN survival compared to the control media. Each condition was replicated in 3–4 independent cultures.

Reactive oxygen species (ROS) production assay

Intracellular ROS levels were measured as previously described by our laboratory (Rojas et al. 2015). Briefly, a stock of 5 mM of the CM-H2DCF-DA probe (Invitrogen, Cat. No.C6827) was prepared fresh in DMSO and then diluted in the culture medium to a final concentration of 1 µM. Cells were washed with PBS 1X to remove the different MCMs for 90 min after applying the different conditioned medium and the CM-H2DCF-DA probe for 30 min at 37 ℃ in the dark. To facilitate the incorporation of the probe into cells, 0.004% pluronic acid F-127 (Invitrogen, Cat. No. P-3000MP) was added. After incubation, the probe CMH2DCF-DA dissolved in the culture media was removed, and cells were washed twice with PBS 1X to apply the culture medium to the spinal cord neurons. Cultures were also incubated with H_2O_2 (200 µM for 20 min) as a positive control to normalize the number of cells with CM-H2DCF-DA signal after the insult with MCMs. Imaging was made using an epifluorescence microscope (Nikon Eclipse Ti-U; objective 20X) and excitation and emission wave λex/λem = 492–495/517–527 nm. At least three fields were taken for each condition, and at least ten cells per field were used for the quantification. The analysis of images was done using ImageJ software (NIH, Bethesda, MD, USA). For quantification purposes, we focused on parameters that are typical for MNs in spinal cord cultures: neurons that display a large soma (> 20 µm diameter) and express five or more primary dendrites. In previous studies, we show that such MN-like cells are triple stained for ChAT, SMI-32 and MAP2 and display characteristic electrophysiological properties (Fritz et al. 2013; Arredondo et al. 2022).

Phosphorylated c-Abl (c-Abl-P) immunofluorescence labeling

c-Abl phosphorylation in MNs was determined by immunofluorescence labeling as previously described (Rojas et al. 2014). Briefly, primary spinal cord cultures were exposed to the different MCMs, fixed at 7 DIV with 4% PFA, and incubated with antibodies against SMI32. To detect phosphorylated c-Abl, a mouse monoclonal antibody that recognizes phosphorylation of Tyr-412 was used and visualized with the appropriate Alexa fluorescent secondary antibody (see Sect. "Immunofluorescence" immunofluorescence). For c-Abl-P quantification in cultures, cultures were imaged using a 20X objective. The fluorescence intensity was quantified in $SMI32^+$ MNs using ImageJ software (NIH, Bethesda, MD, USA). Briefly, the cell body of each $SMI32^+$ neuron was marked manually to set a region of interest (ROI), and the mean c-Abl-P fluorescence was quantified. The background was subtracted, choosing a region without cells. The fluorescence corresponding to control cells was normalized to 1.

Microfluidic system

We used microfluidic chambers with 450 µm long microchannels (Xona, No. SND450). The sterile chambers were mounted on glass coverslips previously treated with poly-L-lysine for 30 min at 37 ℃. Chambers were incubated at 80 ℃ for 1 h to allow the correct adhesion between the chamber and the glass. Chambers were then exposed to UV light for 5 min for sterilization. 100 µl of the medium was applied to each chamber, and MNs were plated (adapted from (Southam et al. 2013)).

MN and myotube co-cultures

Enriched MN cultures for microfluidic experiments were performed as described previously (Milligan and Gifondorwa 2011) with some modifications. Briefly, P0-P1 wild-type mice pups were euthanized by decapitation, the skin on the back removed, and the spinal cord was taken, opening each vertebra right down the middle. The spinal cord was left in cold 1X PBS and subsequently transferred to the digestion solution: Papain (Sigma, No. P3375), DNAase I (Roche, No. 10104159001), MgCl2 (Sigma, No. M2393), 1 ml PBS 1X. Spinal cords were mechanically disaggregated using tweezers, leaving pieces of approximately 0.3 mm, then incubated at 37℃ for 10 min, to be later transferred to a 15 ml tube and washed three times by adding 1X PBS. The spinal cord pieces were placed in 5 ml of preheated MN medium: Neurobasal Medium (Gibco, No. 21103–049), 1% Glutamax (Gibco, No. 35050–061), 2% Supplement B27 (Gibco, No. 17504–04), 5% of horse serum), and DNAase and $MgCl_2$. Then, the spinal cords were disintegrated using glass Pasteur pipettes previously flamed at the tip with two different thicknesses, passing each spinal cord through the pipettes from the greater to the smaller hole. To purify the MNs, an Optiprep gradient column was assembled (Milligan and Gifondorwa 2011). Cells were centrifuged at 1900 rpm for 15 min. After centrifugation, the third layer of the generated gradient, which contains a higher proportion of MNs was removed. The cells were left in a new 15 ml tube with 10 mL of prewarmed MN medium and were centrifuged at 1000 rpm for 10 min. The pellet was carefully resuspended in no more than 200 µl of preheated MN medium, and cells were counted and diluted up to 1×10^6 cells/ml. Approximately 5×10^4 cells were plated in the proximal compartment in no more than 50 µl of MN medium. Cells were incubated for 30 min at 37℃ and 5% CO2 for cell adhesion. Subsequently, 200 µl of MN medium was applied to the culture of MN localized in the upper proximal compartment. The culture medium was replaced every 48 h. At 3 DIV, the first axonal prolongations were observed, and that was the time that the myoblasts were plated in the distal compartment. Like MNs, 5×10^4 myoblast cells from the protocol described before (see Sect. "Myoblasts and myotubes cultures" myoblasts and myotubes cultures) were resuspended in 50 µl of myoblast growth medium and plated in the upper distal compartment. The chamber was incubated for 30 min at 37℃ and 5% CO2, and finally, 200 µl of myoblast growth culture medium was applied in the upper distal compartment. The next day, the medium was replaced to differentiate myotubes to induce fusion of the myoblasts. Approximately between 10 and 14 DIV, it was possible to observe the innervation of MN axons to the distal compartment where the myotubes were cultured.

Adeno-associated viral particle production and titration

Based on previous work (Bustos et al. 2017; Arredondo et al. 2022) HEK293FT cells were grown on 150 mm plates in DMEM medium (Hyclone, SH30081.02) until reaching 80–90% of confluence and supplemented with 10% fetal bovine serum (FBS; Hyclone, SH30070.01), 4 mM L-glutamine (Life technologies, 25,030–081), 100 U/ml penicillin/streptomycin (Life technologies 15,070–063) and 1 mM pyruvate (Sigma), at 37 ℃ and 5% CO2. Cells were transfected using polyethyleneimine (PEI), and the plasmids for adeno-associated viruses type 1 and 2 (pAAV1 and pAAV2) were utilized. In addition, we use the pFΔ6 plasmid and the following plasmids of interest: hSyn-COX8-RFP, a plasmid with the synapsin-1 promoter that controls the expression of COX8, exclusive from mitochondria, and fused to the red fluorochrome RFP; hSyn-mRuby2-GCaMP6, a plasmid with the synapsin-1 promoter that controls the expression of the

biosensor GCaMP6 and fused to the red fluorochrome mRuby2 (Addgene, # 50,942); and hSyn-HyPer, HyPer biosensor 3.0 under CMV promoter (Addgene, #42,131). We transfected 10.4 µg of pFΔ6, 4.35 µg of pAAV1, 4.35 µg of pAAV2, 5.2 µg of the plasmid of interest and 880 µl of Optimem (Gibco, No. 31985–070). Plasmids were mixed, and 260 µl of polyethyleneimine reagent (PEI; Sigma, No. P3143) was added. The solution was applied on 80% confluent HEK293T cells, and after 12 h, the medium was replaced by DMEM medium with 1% FBS. At 72 h from the start of the transfection, cells were collected and centrifuged at 3000 RPM for 10 min 4 ℃. The supernatant was discarded, and the pellet was resuspended in 4 ml 1X PBS. Cells in suspension were left at -80℃ for 10 min and then thawed at 37℃ for 10 min. This cycle was repeated three times to achieve thermal lysis of the cells. Finally, the supernatant was removed and filtered using 1.2 µm, 0.45 µm and 0.22 µm filters. The solution containing the viral particles was aliquoted and refrigerated at -80℃.

AAV particle titration was performed based on previous published protocols (Aurnhammer et al. 2012; Bustos et al. 2023). Briefly, we prepared dilution of the standard plasmid (Addgene, #59,462) from 2×10^9 up to 2×10^3 in nuclease-free H_2O. We also prepared 10 serial dilutions (dilution factor 5x) of the AAV samples in H_2O. We performed a qPCR using the universal SYBR green mix 2x (Thermo Fisher, A25742), and the pair of primers fwd: 5'-GGAACCCCTAGTGATGGAGTT and rev: 5'-CGG CCTCAGTGAGCGA. The working concentration for the viruses was adjusted to 10^6 particles/µl for all the experiments.

Mitochondrial velocity assay

Microfluidic co-cultures of MNs and myotubes were transduced at 10–14 DIV in the proximal compartment using AAV1/2 coding for hSyn-COX8-RFP. 4–7 After transduction (14–21 DIV of co-culture), it was possible to observe the expression of RFP with a mitochondrial pattern in MN under epifluorescence microscopy. At this point, the culture medium was replaced by the different MCMs, and 24 h later the registration of the mitochondrial movement was measured. The microfluidic chamber was placed in a CO_2 chamber (Tokai-Hit) coupled to an epifluorescence microscope (20X objective; Nikon TE-2000). Sequential images of 10 axons per condition that crossed the microchannels in direct contact with myotubes were recorded. The images were acquired every 2 s for 5 min to generate a pattern of the mitochondrial movement. The images were processed in the ImageJ software using the Kymograph plugin. The slopes obtained by Kymograph represent mitochondrial velocity (Zahavi et al. 2015).

Analysis of calcium events in MNs

Co-cultures of MNs and myoblasts were generated in the microfluidics chambers as described above. Next, cells in the proximal compartment containing the MNs were infected with AAV1/2 containing hSyn-mRuby2-GCaMP6s, which encodes for the GCaMP6s biosensor to detect intracellular calcium fluctuations (Chen et al. 2013).After 5–7, DIV of transduction, calcium frequency recordings were performed using an epifluorescence microscope (Nikon TE2000e, 20X objective, and Andor Zyla camera 5.5). Images were taken every 50 ms for 1–1.5 min with an excitation wavelength of 480 nm and emission of 510 nm. The soma of an isolated MN was selected to quantify the frequency of calcium events. Images of the isolated soma were analyzed using the ImageJ software and the Z-Profiler tool, which provides an intensity profile during the time. Each intensity peak was counted manually and was divided by 1 min, resulting in a value expressed as events per min.

Analysis of ROS production in MN in the microfluidic system

Co-cultures of MNs and myoblasts were generated in the microfluidics chambers as described above. Next, cells in the proximal compartment containing MNs were infected with AAV1/2 containing the hSyn-HyPer 3.0 plasmid, which encodes for the HyPer biosensor and YFP protein (Bilan et al. 2013). After 5–7 DIV of transduction, ROS production recordings were performed using an epifluorescence microscope, with an excitation wavelength at 480 nm and emission at 510 nm. Acquisition was made every 2 s for 10 min. Images were analyzed using the ImageJ software, using the Z-Profiler tool to obtain the intensity profile over time.

Data analysis

Statistical analyses were performed using GraphPad Prism software. Student's t-test was performed when two populations were examined, while one-way ANOVA followed by the Bonferroni post-hoc was utilized when making multiple (three or more) comparisons. In all figures, data is reported as mean ± S.E.M.; $^*p<0.05$, $^{**}p<0.01$, $^{***}p<0.001$ compared to control. For all data, three or more independent experiments were analyzed.

Results

MutSOD1 myotubes acquire aberrant phenotypic and functional characteristics

We first aimed to determine the phenotypic characteristics of mutSOD1 myoblasts and myotubes primary cultures. Primary myoblast cultures were generated from lower limb skeletal muscles derived from postnatal day (P) 1–4 neonatal ALS transgenic mice carrying human

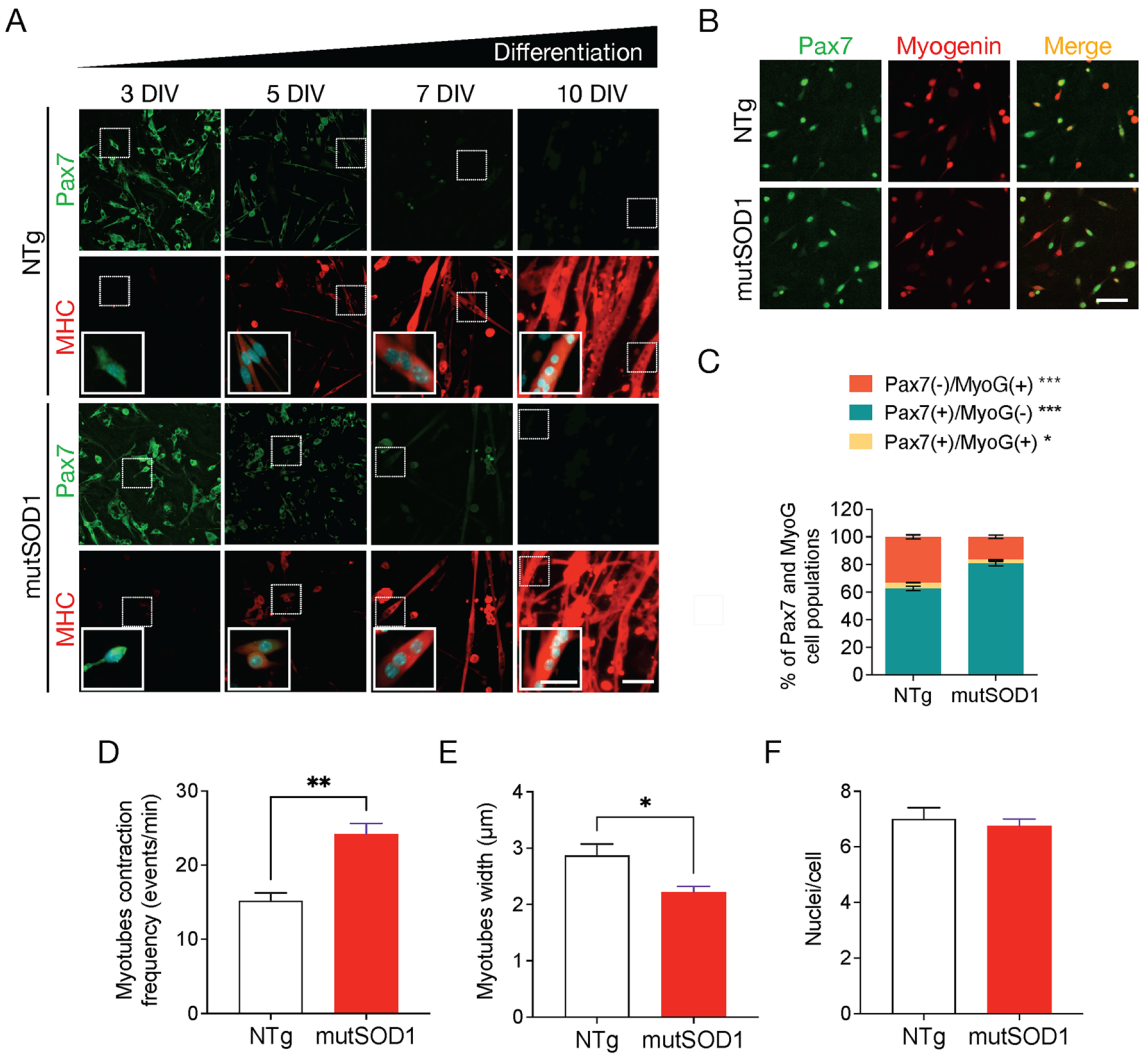

Fig. 1 Characterization of primary mutSOD1 myoblast cultures. **A** Representative images of myogenic markers during myoblast differentiation in primary mutSOD1 and non-transgenic littermate (NTg) myoblast cultures. Myoblasts from P2 mice were maintained in a growth medium up to 70% confluence and then cultured in a differentiation medium to induce myotube formation. Cells were fixed at 3, 5, 7, and 10 DIV and immunostained with antibodies against Pax7 (green) and MHC (red), and DAPI (cyan) to detect nuclei (n = 3). Scale bar: 100 µm; inset: 50 µm. **B** Representative images of myoblast subpopulations present in primary NTg and mutSOD1 myoblast cultures. Five DIV primary mutSOD1 and NTg myoblasts were induced to differentiate into myotubes for 8 h. Cells were fixed, and immunofluorescence was performed using specific antibodies against Pax7 and myogenin (MyoG). Scale bar: 100 µm. **C** Pax7, and myogenin-positive (and negative) cells were quantified to obtain the enrichment percentage of each myogenic gene over the total number of cells. The quantification corresponds to 3 independent experiments, analyzed by student t-test (* $p < 0.05$, *** $p < 0.0005$). **D** Myotube contraction frequency, comparing NTg and mutSOD1 myotubes and quantified as event per min. Data are represented as the mean ± s.e.m., student t-test (** $p < 0.005$). **E** Myotube width. Comparison made between NTg and mutSOD1 myotubes in 3 independent experiments. Data are represented as the mean ± s.e.m., student t-test (** $p < 0.005$). **F** Number of nuclei per cell in NTg and mutSOD1 myotubes. The quantification corresponds to three independent experiments, analyzed by student t-test. No significant differences were detected

mutant SOD1^{G93A}. As controls, myoblasts were isolated from non-transgenic littermates (NTg). Using immunofluorescence staining assays for Pax7 and myosin heavy chain (MHC), we tested the differentiation of myoblasts to myotubes. Pax7 is a transcription factor involved in the early stages of myogenesis, and is essential for the normal expansion and differentiation of satellite cells (SCs) into myoblasts in both neonatal and adult myogenesis (Maltzahn et al. 2013), while MHC is a major component of muscle fibers and a marker for functional myotubes (Torgan and Daniels 2001; Guo et al. 2020b). At 3–5 DIV, when NTg and mutSOD1 myoblasts reached 70% confluence, we observed a robust expression of the transcription factor Pax7 (Fig. 1A). Next, differentiation

media was applied to induce complete fusion and differentiation to myotubes. As expected, during the differentiation process the expression of Pax7 decreased concomitantly with an increased expression of MHC (Fig. 1A). Both NTg and mutSOD1 cultures displayed myoblast to myotube transition over ten days. Next, we analyzed the efficiency of the myotube formation by performing a short differentiation assay (8 h) followed by double immunofluorescence assays to determine the expression of both Pax7 and myotube marker myogenin (MyoG) (González et al. 2016). MyoG is a key transcription factor that plays a crucial role in the terminal differentiation of myoblasts into myotubes in vitro, and muscle fibers in vivo (González et al. 2016). Interestingly, mutSOD1 myotubes showed a significant reduction (~ 50%) in myogenin induction ($Pax7^{-}/MyoG^{+}$) compared to NTg myotubes, indicating a deaccelerated commitment to myotube differentiation (Fig. 1B-C). To further characterize the myogenic process in the ALS cells, we analyzed the structural and functional traits of NTg and mutSOD1 myotubes. Since myotube cultures show spontaneous contractions (Guo et al. 2013; Smolina et al. 2015), we analyzed the contraction capability in our model. We found that mutSOD1 myotubes displayed a significantly higher contraction frequency (~ 55%), compared to NTg myotubes (Fig. 1D). Moreover, we determined that mutSOD1 myotubes display a significantly lower width (~ 23%), compared to NTg myotubes (Fig. 1E), without evident changes in nuclei number per myotube (Fig. 1F). Together, these results show that mutSOD1 myotubes display intrinsic phenotypic and functional differences compared to NTg muscle cells.

Exposure to mutSOD1-MCM triggers the death of primary MNs

Next, we aimed to explore the hypothesis that skeletal muscle expressing mutSOD1 causes MN pathology and death by releasing soluble toxic factor(s). We established an in vitro culture model (Fig. 2A) in which myotube-conditioned media (MCM) from mutSOD1 myotubes (termed mutSOD1-MCM) was applied at different dilutions to ventral spinal cord cultures at 4 DIV. The equal dilutions in both the NTg-MCM and mutSOD1-MCM enable to determine whether reduction of MN survival is through gain-of-toxicity or loss-of-support mechanisms. MCM from NTg astrocytes (termed NTg-ACM) and fresh media to maintain MNs in culture (termed MN medium) were included as controls. At 7 DIV, cultures were fixed and double immunostained for unphosphorylated neurofilament-H (SMI32) and MAP2 to identify MNs ($SMI32^{+}/MAP2^{+}$-cells) or interneurons ($SMI32^{-}/MAP2^{+}$-cells) (Nagai et al. 2007; Sepulveda et al. 2010; Fritz et al. 2013; Mishra et al. 2020; Arredondo et al. 2022). In agreement with our hypothesis and a gain-of-toxicity mechanism, we found that a 1/4 (25%) and 1/8 (12.5%) dilution of mutSOD1-MCM strongly reduced MN survival (~ 40–50%), whereas NTg-MCM did not cause MN death (Fig. 2B-C). Using the same mutSOD1-MCM dilutions, we did not observe changes in the survival of interneurons (data not shown), although we cannot discard that these neurons contribute to ALS pathology.

In a separate set of experiments, we fractioned the different MCMs using 10 kDa filters. We found that only mutSOD1-MCM fractions under 10 kDa (dilution 1:4) displayed a toxic effect that was associated to a reduction in 40% the MN survival (supplemental Fig. 1). In order to gain a deeper insight of the possible size of the toxic factor within mutSOD1-MCM, we also used Size Exclusion Chromatography (SEC) to further fraction both < 10 kDa NTg- and mutSOD1-MCMs. We found that the first fractions 1–11, but not fractions 12–18, caused MN death, suggesting that particular small molecules, metabolites and small peptides, in mutSOD1-MCM display toxicity to MNs (Supplemental Fig. 1).

Application of mutSOD1- MCM to spinal cord cultures leads to increases in ROS/RNS and c-Abl-P

To further analyze possible cellular mechanisms underlying MN death induced by mutSOD1-MCM, we focused on two classical pathogenic events reported in MNs in ALS models, namely accumulation of reactive oxygen species (ROS)/reactive nitrogen species (RNS) and activation of c-Abl (Marchetto et al. 2008; Fritz et al. 2013; Rojas et al. 2014, 2015). Based on our previous time-course imaging studies measuring ROS/RNS and c-Abl-P in spinal cord neurons induced by mutSOD1 astrocyte-conditioned media (Rojas et al. 2014, 2015), in the current study we applied mutSOD1-MCM for 90 min to 4 DIV spinal neurons for both sets of experiments. NTg-MCM and MN media were used as negative controls (90 min), and H_2O_2 (200 µM, 20 min) was used as positive control. To investigate whether mutSOD1-MCM leads to increases in intracellular ROS/RNS levels, following incubation, spinal cord neurons were washed and loaded for 30 min with CM-H_2DCF-DA. This non-fluorescent dye passively diffuses into cells, but upon hydrolysis, the generated DCFH carboxylate anion is trapped inside the cells where oxidation leads to the formation of the fluorescent product DCF. The increased DCF fluorescent intensity reflects the accumulation of certain ROS/RNS species. Using combined real-time fluorescence and phase-contrast imaging, a substantial increase in intracellular DCF fluorescence was observed upon application of MCM-mutSOD1 diluted 1/4 in spinal cord neurons, including in MN-like cells (Fig. 3A). Further dilutions of

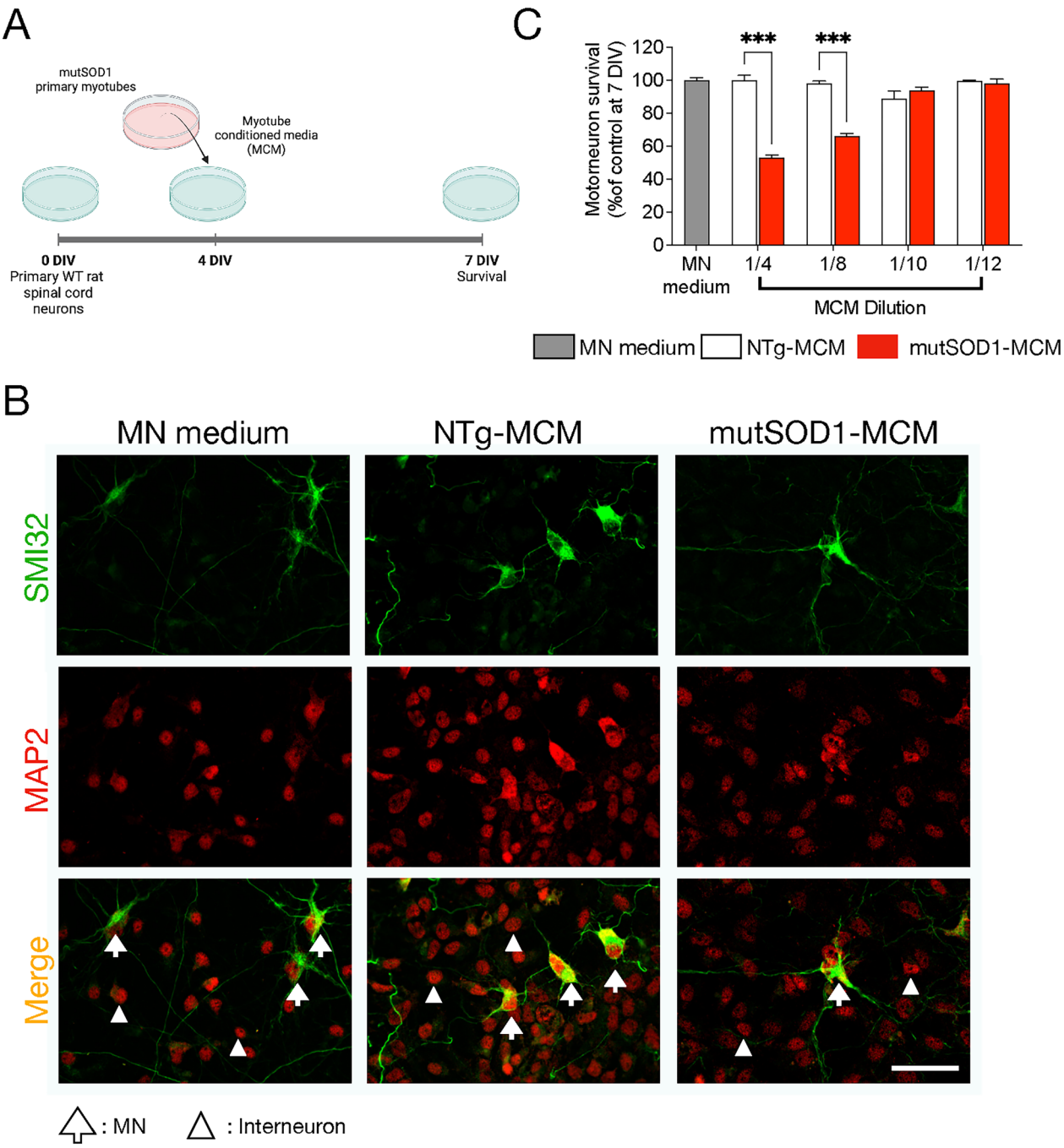

Fig. 2 MCM-mutSOD1 contains soluble toxic factor(s) that induce(s) MN death. **A** Workflow diagram of primary WT (NTg) spinal cord cultures (4 DIV) that were exposed for 3 days to MCM derived from mutSOD1 transgenic mice (MCM-mutSOD1), NTg littermates (NTg-MCM), and culture medium (MN medium). Cells were fixed at 7 DIV, and immunofluorescence assayed cell survival. **B** Representative images of immunofluorescence against SMI32 (MNs; green) and MAP2 (all neurons; red) when exposed to MCM-mutSOD1 (dilution 1/4), NTg-MCM (dilution 1/4), and MN medium. Scale bar: 50 µm. **C** MN survival graph ($SMI32^+/MAP2^+$ cells as a percentage of all $MAP2^+$ neurons) after treatment with MCM-mutSOD1, NTg-MCM, and MN medium for 3 DIV. Values represent the mean ± s.e.m of at least three independent experiments performed in duplicate and analyzed by one-way ANOVA (*** $P < 0.0005$) relative to the NTg-MCM at 7 DIV

1/8 MCM-mutSOD1 produced an increase in intracellular DCF (Fig. 3B). This effect disappears after dilutions 1/10 of MCM-mutSOD1 (Fig. 3B). The application of H_20_2 mimicked this increase in DCF labeling. In control conditions, NTg-MCM and MN media did not change intracellular DCF levels (Fig. 3A-B).

Using immunolabeling, we next evaluated the effect of mutSOD1-MCM on the levels of phosphorylated c-Abl kinase (c-Abl-P), a tyrosine kinase widely associated with neuronal apoptosis, activated under a wide range of stimuli including inflammation, DNA damage, amyloid beta, and oxidative stress (Etten 1999; Tsai and Yuan 2003; Wang 2005; Klein et al. 2010; Schlatterer et al. 2011; Yáñez et al. 2016; Martinez et al. 2023). After 90 min of application of the media, cells were fixed and double immunostained with an antibody against SMI32 to identify MNs and with a specific antibody that recognizes c-Abl that is phosphorylated on tyrosine 412 (Tyr412), a site that enhances c-Abl catalytic activity (Hantschel and Superti-Furga 2004). We detected a significant induction of c-Abl-P in MNs incubated with 1/4 dilution of MCM-mutSOD1 compared to controls NTg-MCM or MN media (Fig. 3C-D). Together, these results indicate that soluble toxic factor(s) released by myotubes that carry mutSOD1 lead to increases in ROS/RNS and c-Abl-P in MNs.

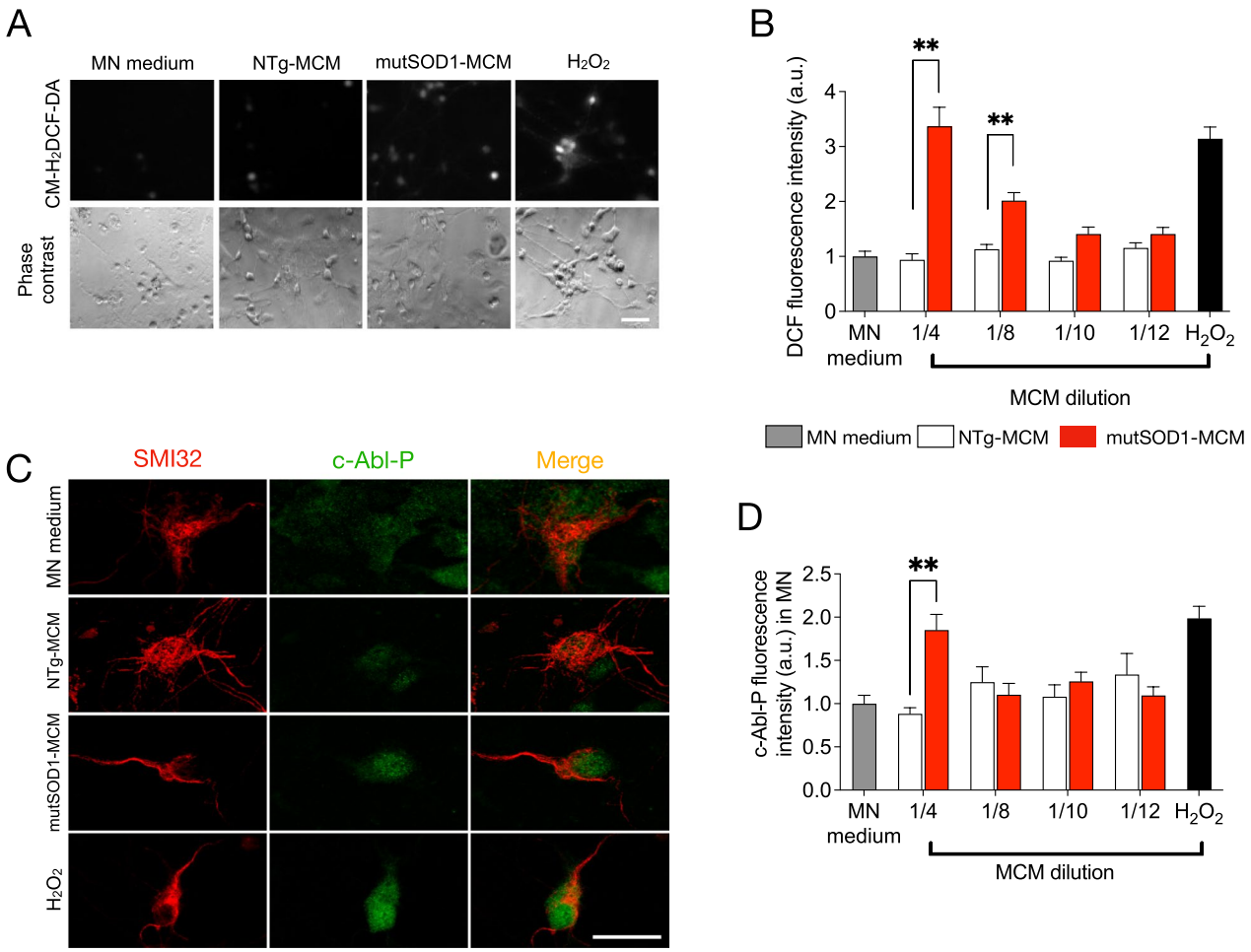

Fig. 3 MCM-mutSOD1 triggers phosphorylated c-Abl and H_2O_2 accumulation. **A** Representative images of DFC assay and phase contrast of NTg spinal cord cultures exposed to MCM-mutSOD1 (dilution 1/4), NTg-MCM (dilution 1/4), MN medium, and H_2O_2 (200 mM) as a positive control. Scale bar: 50 µm. **B** Graph of the average intensity of DFC probe in neurons treated for 90 min with MCMs at different dilutions, as indicated. The graph represents the average ± s.e.m of three experiments performed independently and analyzed by one-way ANOVA (**, $P < 0.005$ relative to NTg-MCM. **C** Representative images of immunofluorescence against phosphorylated c-abl (c-Abl-P; green) and SMI32 (MNs; red) when exposed for 90 min to MCM-mutSOD1 (dilution 1/4), NTg-MCM (dilution 1/4), and MN medium, and H_2O_2 (200 mM, 20 min) as a positive control. Scale bar: 50 µm. **D** Graphs showing fluorescence intensities (a.u.) for c-Abl-P at 4 DIV when NTg spinal cord cultures were treated acutely (90 min) with MCM at different dilutions, as indicated. The graph represents the mean ± s.e.m of three experiments performed independently and analyzed by one-way ANOVA (** $P < 0.005$) relative to the NTg-MCM

MutSOD1-MCM induces MN death distally through the axons

Muscle-motoneuron communication is key for maintaining the NMJ and for the long-term survival of MNs (Ionescu et al. 2016). Alterations in intracellular communications can lead to synapse disruption and axon degeneration, which could be an inflection point in neurodegenerative diseases, including ALS (Maimon et al. 2018). The molecular signaling for the correct maintenance of neuromuscular communication can act locally at the synapse or travel long distances through the axon by retrograde transport. In our previous survival experiment (see Fig. 2), the MN soma and the axon are in direct contact with the MCM. Therefore, it is not possible to determine if the observed effects of myotube-derived toxic factor(s) on MN survival exert their impact in the soma (proximal effect) or through the axons (distal effect). For this reason, we used microfluidic devices that enable a physical separation between the neuronal soma and its synaptic terminal, with no fluid exchange between the chambers. Primary MNs from neonatal wild-type mice were cultured in the microfluidic devices in the proximal compartment (Fig. 4A, B). At 4 DIV, MCM 1/4 dilution was applied in the distal compartment (Fig. 4B). After three days, cells were fixed and immunostained for SMI32 and MAP2 to determine MN survival (Fig. 4C). To evaluate the survival of MNs more precisely, the MN compartment was divided into two sides (sides A and B; Fig. 4A), separating the MNs that were further from the microchannels, which were less likely to have direct contact with the MCMs (termed non-innervating side A) from those MNs closer to the microchannels and hence more likely to have innervated the distal chamber and thus directly contact the conditioned environment (termed innervating side B) (Fig. 4C). We found that distal application of mutSOD1-MCM reduced MN survival by 30% in the cell located in innervating side B, while no significant MN loss was detected in non-innervating side A (Fig. 4C-E). Moreover, we found that neither NTg-MCM nor MN media reduced MN survival on either side A or B (not shown). Together, these results indicate that the toxic factor(s) present in the mutSOD1-MCM exerts its effect retrogradely.

Distal application of mutSOD1-MCM increases Ca^{2+} transients in wild-type MNs

Next, we wanted to get insights into molecular mechanisms that underlie the mutSOD1 myotube-mediated toxicity on MNs through a retrograde manner. To recreate the MN-muscle communication, and to ensure the generation of abundant functional MN axons in this distal chamber, WT (NTg) myotubes were grown in the distal compartment (Fig. 5A). Regarding potential mechanisms, we first focused on measuring intracellular Ca^{2+} transients as abnormalities in Ca^{2+} homeostasis has been implicated in the disruption of kinesin-mediated axonal trafficking (Li et al. 2004; Hollenbeck and Saxton 2005). To determine if mutSOD1-MCM causes alterations in intracellular Ca^{2+} transients in the MNs, we used the GCaMP6 sensor to transduce the proximal MN compartment of the microfluidic devices (Rose et al. 2016). Seven days after transduction, we replaced the medium for MN media, NTg-MCM, or mutSOD1-MCM in the proximal and distal chambers (Fig. 5A). Five min later we recorded the MN somas for 2 min to analyze Ca^{2+} events. Independent of the chamber used, low MN activity (5–7 spontaneous Ca^{2+} events/min) was measured when MN media (control) or NTg-MCM was applied (Fig. 5B–C). By contrast, application of mutSOD1-MCM in the proximal chamber led to a significant increase of 2.5-fold (~12 events/min) in transient Ca^{2+} events (Fig. 5B). When adding mutSOD1-MCM in the distal chamber, we observed an even higher increase of 3–4 fold (~20 events/min) in transient Ca^{2+} events (Fig. 5C). These results show that soluble factor(s) released from mutSOD1 myotubes trigger an increase in Ca^{2+} transients, particularly when applied at the axonal compartment where the NMJ resides, suggesting a distinct spatial effect of toxic mutSOD1-MCM.

mutSOD1-MCM applied distally induces H_2O_2 accumulation in wild-type MNs

Studies in ALS-related SOD1 mutations indicate that mitochondrial dysfunction participates in the pathogenesis of MNs through the generation of intracellular ROS (Barber and Shaw 2010; Rojas et al. 2014, 2015; Vehviläinen et al. 2014). As reported with DCF (Fig. 3), mutSOD1-MCM triggers an accumulation of ROS/RNS in WT (NTg) spinal cord cultures. To evaluate whether mutSOD1-MCM can induce ROS accumulation in MNs in a distal and retrograde manner in the microfluidic cultures, we used the HyPer-3 probe as a biosensor for intracellular H_2O_2 in living cells (Bilan et al. 2013). Co-cultures of wild-type myotubes and MNs were generated, with the latter neuronal compartment transduced with AAV1/2-HyPer-3. Seven days after transduction, NTg-MCM or mutSOD1-MCM was applied to the distal chamber (Fig. 5D-E), and serial images were taken in an epifluorescent microscope (every 2 s for 6 min). We found that the application of mutSOD1-MCM significantly increased ~2.5-fold the HyPer-3 fluorescent intensity relative to NTg-MCM (Fig. 5E–F). These results show that applying mutSOD1-MCM to the axonal compartment triggers the accumulation of intracellular H_2O_2 levels in MN somas.

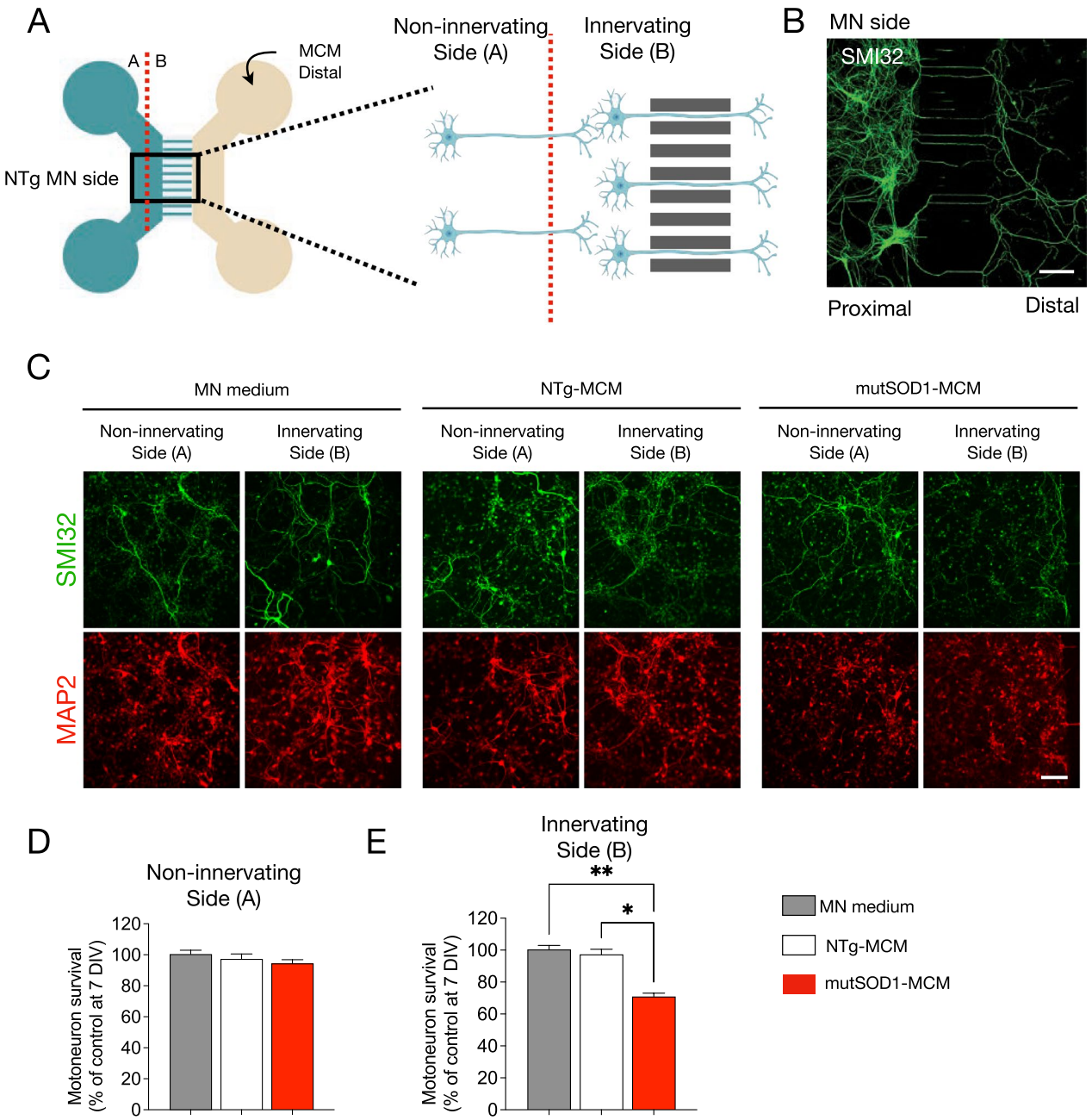

Fig. 4 MN survival is reduced in microfluidic systems when exposed to mutSOD1-MCM. **A** Representative diagram showing a microfluidic device to determine the survival of primary NTg MN cultures (cultured on MN side) at 14 DIV under the distal application of MN medium, NTg-MCM and MCM-mutSOD1 for 3 DIV: indicated is the non-innervating (side A) and non-innervating (side B) of MNs. Next, MNs were fixed and incubated with specific antibodies against SMI32 to detect MNs and total nuclei visualized with NucBlue staining to obtain the ratio between MNs and total cells. **B** Immunostaining against SMI32 in 3 DIV NTg primary MN culture in a microfluidic device. Cells were plated in the proximal compartment and MCM-mutSOD1 was applied in the distal compartment for survival quantification. Scale bar: 200 µm. **C** Representative images of immunofluorescence against SMI32 (MNs; green) and MAP2 (all neurons; red) when exposed to MN medium, NTg-MCM, and MCM-mutSOD1 in the non-innervating (side A) and non-innervating (side B) of the proximal chamber. In none of these conditions, we observed a significant difference in the number of axons crossing the microfluidic slit. Scale bar: 100 µm. **D** Quantification of survival of non-innervating MN after distal treatment with MN medium, NTg-MCM and MCM-mutSOD1 in a microfluidic chamber. Values represent the mean ± s.e.m. of three independent experiments and analyzed by one-way ANOVA relative to the NTg-MCM at 17 DIV. **E** Graph of survival of innervating MN after distal treatment with MN medium, NTg-MCM and MCM-mutSOD1 in the microfluidic chamber. Values represent the mean ± s.e.m. of three independent experiments and were analyzed by one-way ANOVA (*P < 0.05 **P < 0.005) relative to the NTg-MCM relative to the control medium at 17 DIV

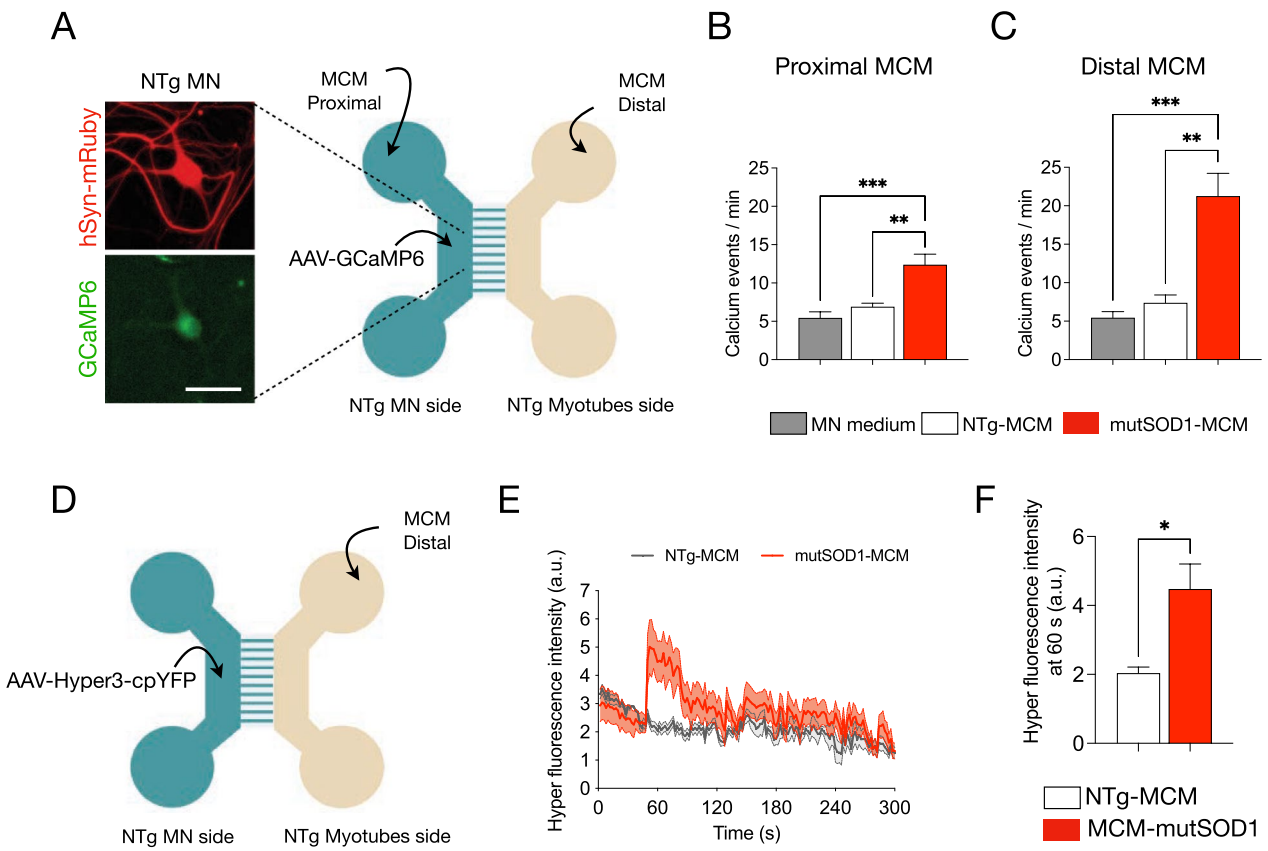

Fig. 5 Application of mutSOD1-MCM rapidly increases calcium transients and induces H_2O_2 accumulation in wild-type MNs. **A** Representative diagram of NTg MNs and NTg myotubes co-cultured in a microfluidic chamber. Images show examples of MN that were subjected to transduction with AAV1/2-hSyn-mRuby2-GCaMP6s (titer 10^6 particles/µl; hSyn-mRuby in red, and GMaMP6s in green, left panel). Seven days later, cultures were exposed to NTg-MCM and MCM-mutSOD1 in the myotube (distal) or MN (proximal) compartment for 10 min before measuring calcium events. Scale bar: 50 µm. **B**, **C** Quantification of the number of calcium events per min of MN exposed to the different MCMs, as indicated. Values of the graph represent the mean ± s.e.m. of three independent experiments and analyzed by one-way ANOVA (** $P < 0.005$, *** $P < 0.0005$) relative to the MN medium and NTg-MCM. **D** Schematic of a co-culture of NTg MNs expressing the Hyper-3 sensor (using the AAV1/2 with titer $10.^6$ particles/µl) and NTg myotubes from P2 mice in a microfluidic chamber, where MCM (NTg and mutSOD1) were applied in the distal myotube compartment. **E** Signal profile plot of Hyper3 fluorescent signal vs. time after application NTg-MCM and MCM-mutSOD1.Values of the graph represent the experimental average of six cells (n = 6), using the same microfluidic chamber, and analyzed by t-student test (*$P < 0.05$) relative to NTg-MCM. **F** Fluorescent intensity of Hyper measured at 60 s from the profile, after application NTg-MCM and MCM-mutSOD1. Values represent the mean ± s.e.m. and analyzed by t-student test (*$P < 0.05$) relative to NTg-MCM (n = 6)

MCM-mutSOD1 affects antegrade and retrograde mitochondrial axonal transport in MNs

To analyze the possibility of an axonal trafficking dysfunction as a pathological cell event, we evaluated the antegrade (from the soma to the axonal terminal) and retrograde (from the axon terminal to the soma) mitochondrial transport in MN-myotube microfluidic co-cultures (Fig. 6A). To visualize MN axons, 3 DIV MNs were transduced with an AAV1/2 harboring a red fluorescent protein (RFP) fused to a mitochondrial targeting sequence Cox8 (Fig. 6A). mutSOD1-MCM or NTg-MCM was applied to the myotube (distal) or MN (proximal) compartments and 24 h later mitochondrial movement in the axons of the MN was recorded. We tracked the mitochondrial axonal movement through the microchannels of the microfluidic chamber, thereby only quantifying axons in contact with the distal compartment. The generated videos were converted to kymograph images representing the movement of a particle over time. The resulting slopes show mitochondrial velocity (Fig. 6C-D). Compared to NTg-MCM, we observed that incubation of mutSOD1-MCM in the proximal compartment (MNs) significantly decreased the mitochondrial velocity of both the antegrade (from 0.55 µm/s to 0.3 µm/s) and retrograde movement (from 0.4 µm/s to 0.3 µm/s) (Fig. 6C, E). Conversely, the application of mutSOD1-MCM to the distal chamber only affected anterograde, but not retrograde transport (Fig. 6D, F). These results indicate that

mutSOD1-MCM affects differentially axonal mitochondrial transport, with the antegrade transport being the most affected by the muscle-released toxic factor(s).

Discussion

The role of muscle in ALS pathology involves complex interactions, including potential contributions to disease progression and the modulation of MN function. Even though the role of skeletal muscle in ALS pathogenesis remains controversial, increasing evidence points out a preponderant non-autonomous mechanism underlying MN degeneration (Dobrowolny et al. 2005; Dupuis et al. 2009; Wong and Martin 2010; Badu-Mensah et al. 2020). To elucidate novel non-autonomous mechanisms of muscle-mediated MN degeneration in ALS, we generated a highly homogenous population of primary skeletal myotubes from myoblasts derived from ALS transgenic mice expressing human mutSOD1 and from control NTg littermates. Characterization of the cultures revealed that mutSOD1 skeletal myoblasts and myotubes display phenotypic and functional differences compared to control cultures. Given that our in vitro ALS muscle model is free of other critical implicated cell types, such as MNs, astrocytes, and microglia, our data suggest that the aberrant phenotypic and functional signature of mutSOD1 myotubes is cell autonomous.

Our results support previous in vitro ALS studies showing impaired myoblast proliferation and differentiation to myotubes (Manzano et al. 2013). Our findings also agree with findings that reported an inhibitory effect of mutSOD1 expression on the myogenic program in C2C12 cells (Martini et al. 2015). Another recent report further suggests a decreased differentiation commitment using a human ALS skeletal muscle model generated from induced pluripotent stem cells (iPSCs) derived from ALS patients harboring mutations in SOD1 and compared to iPSCs from healthy individuals (Badu-Mensah et al. 2020).

On the other hand, the expression pattern of Pax7 and MyoG contrasts with data obtained from skeletal muscle biopsies of symptomatic ALS patients (Jensen et al. 2016). Thus, while we found increased Pax7 and decreased MyoG protein levels in cultured mutSOD1 myotubes, decreased Pax7 and increased MyoG mRNA levels were detected in mutSOD1 skeletal muscles obtained from symptomatic ALS patients. Based on additional data in the same study (comparing baseline with 12 weeks of progression), it was suggested that the activated myogenic process in symptomatic ALS muscle likely intends to overcome the denervation-induced muscle wasting (Jensen et al. 2016). Comparing the data on cultured ALS myotubes with the analysis from skeletal muscle biopsies, it is plausible that compensatory mechanisms during the progress of the disease could cause drastic alterations in myogenesis, changing from a deaccelerated process to an accelerated process. We acknowledge, however, that directly comparing the complex 3D muscle tissue with a 10 DIV 2D culture system is not ideal. 3D muscle tissue develops over weeks to months in symptomatic ALS mice and decades in symptomatic ALS humans and is connected to MNs. Our cultures system, on the other hand, contains a relatively homogeneous population of myotubes and exhibits some characteristic myotube markers but without having formed functional connections to MNs before culturing. To compare the in vitro and in vivo data more meaningfully, it would be essential to characterize from ALS mice specific muscle cell types and conduct longitudinal studies, including at pre-symptomatic stages, and compare these results with ALS myotubes that have been co-cultured with MNs in microfluidic devices.

In our study, we further investigated the contraction frequency of our primary myotubes as a marker of contractile function. While several studies have reported impaired contractile function in mutSOD1 models, most employed electrical stimulation (not measuring spontaneous activity) and focused on adult mouse muscle or primary myotubes co-cultured with MNs (Derave et al. 2003; Dupuis et al. 2004; Wier et al. 2019; Badu-Mensah et al. 2020; Benlefki et al. 2020). Notably, Derave et al. (2003) observed slowed contraction in aged mutSOD1 mice at later stages of disease progression (P90 and P120). In contrast, our study uniquely assessed spontaneous contraction frequency in isolated myotubes derived from neonatal mice. Surprisingly, we found increased

(See figure on next page.)

Fig. 6 MCM-mutSOD1 applied proximally affects both antegrade and retrograde axonal transport. **A** Representative diagram of MN and myotube co-cultures in a microfluidic chamber. MNs were subjected to transduction with AAV1/2-Cox8-RFP (1×10^6 particles/µl). Seven days later, cultures were exposed to NTg-MCM and MCM-mutSOD1 in the MN (proximal) or myotube (distal) compartment for 24 h for mitochondrial recording. **B** Schematic of a kymograph to quantify mitochondria movements. Green lines and arrows indicate anterograde movements (from MN soma to axons), while red lines and arrows indicate retrograde movements (from axons to MN soma). **C**, **D** Representative kymographs of mitochondrial movement in MN axons exposed to the different MCM, as indicated. **E**, **F** Graphs of axonal mitochondrial velocity quantified from generated kymographs when MCM was applied in the proximal (**E**) and distal (**F**) chambers. Values of the graph represent the mean ± s.e.m. of three independent experiments and analyzed by t-Student test (*$P < 0.1$, **$P < 0.01$) relative to NTg-MCM

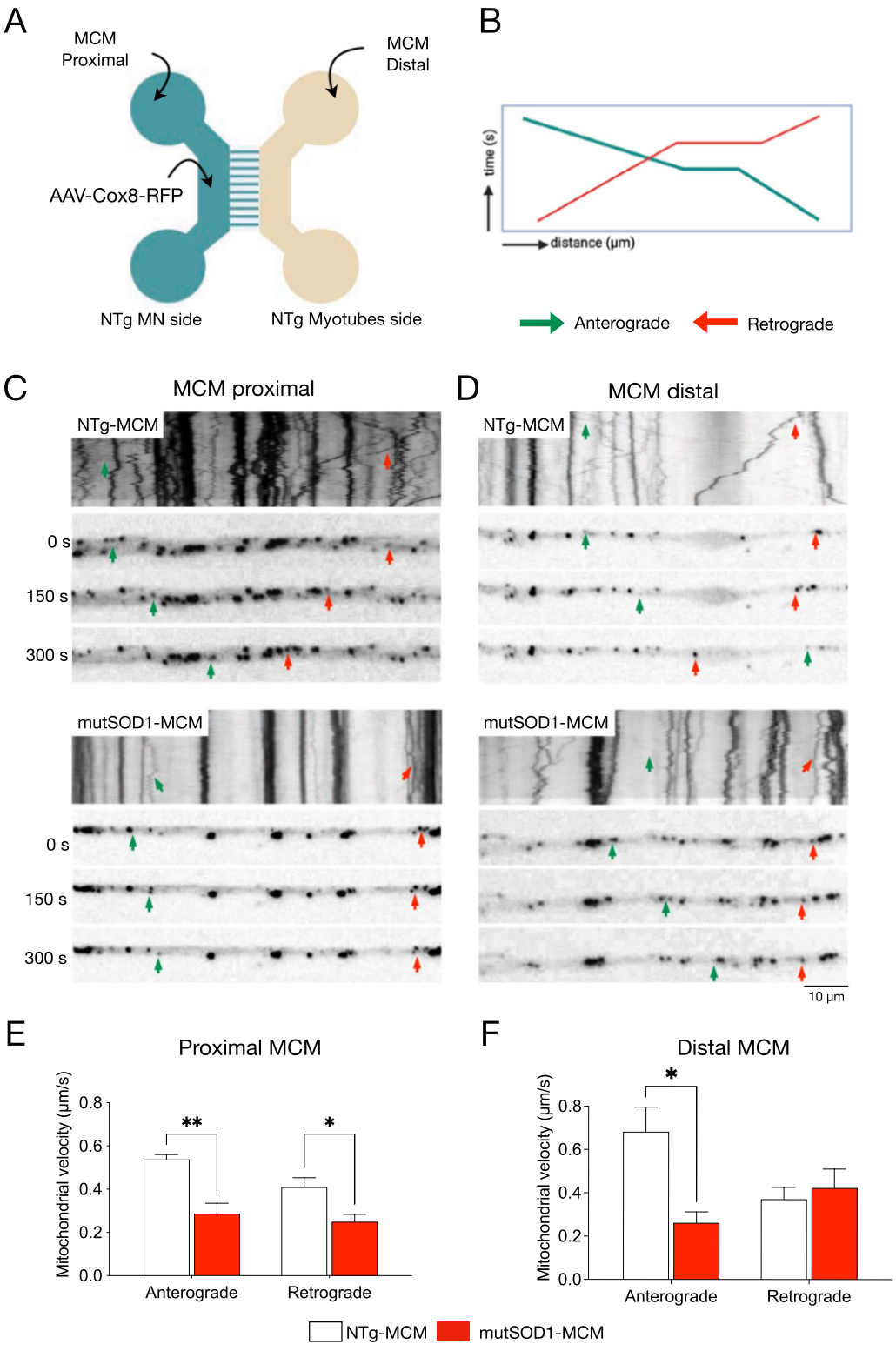

Fig. 6 (See legend on previous page.)

spontaneous contraction frequency in mutSOD1 myotubes compared to controls. This finding is intriguing, considering the delayed maturation observed in our mutSOD1 myotubes. It suggests that altered contractile behavior may manifest early in disease progression, independent of MN influence, and warrants further investigation into the underlying mechanisms.

We also studied how conditioned media derived from mutSOD1 myotubes affects the function and survival of healthy NTg rodent MNs in typical mixed spinal cord cultures and compartmentalized microfluidic chambers enriched in MNs. Our finding that mutSOD1-MCM robustly kills MNs establishes that soluble toxic factor(s) released by ALS myotubes cause non-cell autonomous MN death. Recent metabolome studies using ALS mutSOD1 myocytes revealed alterations in secreted molecules such as amino acids, small molecules (tri- or tetrapeptides), and lipid-based signaling molecules (Stella et al. 2023). Interestingly, our results show that toxic factors secreted from mutSOD1 myotubes are no larger than 10 kDa, suggesting that small molecules, including small peptides, metabolites and/or amino acids, are implicated in the observed MN toxicity. In future studies, it would be important to reveal the identity of small toxic molecule(s) released by ALS myotubes and the underlying molecular mechanisms how these small molecules kill MNs. Given that accumulating evidence suggest that exosomes can contribute to neurodegenerative diseases, including ALS (Iguchi et al. 2016; Tao and Gao 2024), it would be important to test also whether exosome fractions from ALS myotubes can cause MN toxicity.

Applying mutSOD1-MCM to spinal cord cultures further revealed a rapid induction of several classical pathogenic events in MNs, including impaired mitochondrial transport, disturbed calcium homeostasis, oxidative stress accumulation, and cell death induction. The findings underlying the mutSOD1-MCM application support previous observations of MN cell pathology which include impaired axonal transport of mitochondria from muscle to MNs contributing to ALS pathogenesis. Other studies also demonstrate that MNs display disrupted mitochondrial transport, calcium overload, and oxidative stress in diverse ALS mouse models, leading to MN degeneration (Magrané et al. 2012; Rojas et al. 2014, 2015). Furthermore, dysregulation of calcium homeostasis, mitochondria dysfunction and oxidative stress in MNs involves non-cell-autonomous processes by ALS astrocytes, as previously demonstrated by our lab using mutSOD1-ACM (Fritz et al. 2013; Rojas et al. 2014, 2015; Arredondo et al. 2022). The studies with mutSOD1-ACM and mutSOD1-MCM suggest that ALS astrocytes and muscle cells can convergent to a common mechanistic pathological pathway in MNs.

Here we found that soluble factor(s) released by mutSOD1 myotubes exert their toxic effects predominantly retrogradely, causing axonopathy and leading to lethal pathogenic changes. Our present in vitro evidence showing non-cell-autonomous toxic actions of mutSOD1 myotubes to healthy MNs agrees with several studies in vitro and in vivo. Thus, Maimon and colleagues (2018), using a compartmentalized microfluidic co-culture system with wild-type MN explants and primary myocytes, demonstrated that diverse ALS-causing genes, including mutations in SOD1, TDP43, and C9ORF72, promoted axon degeneration. In addition, studies using transgenic mice that express mutSOD1 selectively in skeletal muscles found alterations associated with ALS pathogenesis (Dobrowolny et al. 2009; Wong and Martin 2010; Maimon et al. 2018). Specifically, Dobrowolny and colleagues (2009) showed that muscle-specific expression of mutSOD1 in mice induces severe muscle atrophy accompanied by microglia activation in the spinal cord but without evident signs of MN degeneration. Wong and Martin (2010) found that their transgenic mice exhibiting a skeletal muscle-restricted expression of mutSOD1 also developed muscle pathology and neurologic and pathologic phenotypes consistent with ALS, evidenced by spinal MNs developing distal axonopathy and significant MN degeneration. As indicated in the latter work, the difference between the severity of alterations in the spinal cord observed with the two transgenic studies could be explained by the aging of the animals; thus, Wong and Martin (2010) led their mice to become old, while Dobrowolny et al. (2009) performed their analyses on much younger mice (1–4-month-old) (Dobrowolny et al. 2009; Wong and Martin 2010; Maimon et al. 2018). Despite that these studies support our findings, other in vitro and in vivo studies did not find evidence for a primary role of muscles in ALS. Specifically, in another in vitro study -were conditioned media was generated by mutSOD1 myotubes/myocytes- was unable to reduce the survival of NTg mouse MNs, either analyzed in mixed spinal cord cultures or in cultures enriched for embryonic stem-cell derived MNs (Nagai et al. 2007). While the media was conditioned for seven days in both studies, the reason(s) underlying the difference between their results and ours may be related to technical issues associated with the generation of myotubes. For example, in our study, mutSOD1 myoblasts were differentiated into myotubes in 10 days, a process validated by phenotypic and functional analysis. In the previous study (Nagai et al. 2007), it was reported that myotubes were formed in 2–3 days from myoblasts (without showing characterization), making it plausible that not fully differentiated myotubes

were generated from mutSOD1 myoblasts. Two in vivo studies also indicate that muscle is not a primary target for non-cell-autonomous toxicity in ALS (Miller et al. 2006; Towne et al. 2008). It was shown that delivery of RNA interferences (RNAi) targeting SOD1 to skeletal muscles in the mutant $SOD1^{G93A}$ mouse model did not alter the time of onset of the disease or its progression despite causing a 50–60% reduction in SOD1 protein levels in the examined muscle (Miller and Sheetz 2004; Towne et al. 2008). In both studies, the viral particles (AAV and lentivirus) to deliver RNAi against SOD1 were injected in young adult mutSOD1 mice; thus, intra-muscularly at P40 (Miller et al. 2006) or intravenously at P42 (Towne et al. 2008). Given that systematic studies of hindlimb muscles in mutSOD1 mice revealed functional and structural motor unit loss starting already at P40-P50 (Frey et al. 2000; Fischer et al. 2004; Hegedus et al. 2007; Saxena and Caroni 2011; Zundert et al. 2012), it is plausible that the late viral delivery of SOD1-RNAi to the skeletal muscles was unable to significantly protect and/or revert already induced muscle damage. This would not be surprising as multiple studies designed to reduce mutSOD1 in the CNS revealed that silencing in SOD1 gene expression only was able to significantly delay ALS onset and/or extend lifespan when the treatment was started during early developmental, strongly declining efficacy in maturing mice (Zundert and Brown 2017).

Together, our data presented here, along with previous in vitro and in vivo studies (Dobrowolny et al. 2009; Wong and Martin 2010; Maimon et al. 2018; Badu-Mensah et al. 2020), demonstrate that ALS skeletal muscle causes MN death and classic pathogenicity through non-cell-autonomous processes. Identifying the factors released by ALS skeletal muscle that are toxic to MNs will be essential to translate this knowledge into muscle-targeting treatments for ALS.

Supplementary Information

The online version contains supplementary material available at https://doi.org/10.1186/s10020-024-00942-4.

Supplementary material 1: Figure S1. Small molecules <10 kDa from mutSOD1-MCM are responsible for MN death. A, MN survival graph (SMI32+/MAP2+ cells as a percentage of total MAP2+ neurons) after treatment for 3 days with MN medium, NTg-MCM, MCM-mutSOD1, and both NTg-MCM and MCM-mutSOD1 when passed through >10 kDa and <10 kDa filters. Values represent the mean ± s.e.m of at least three independent experiments and analyzed by one-way ANOVA (*** P <0.001). B, MN survival graph (SMI32+/MAP2+) after treatment for 3 days with MN medium, NTg-MCM, MCM-mutSOD1, and both <10 kDa filtered NTg-MCM and MCM-mutSOD1 when further passed through a Size Exclusion Chromatography (SEC). Results from 2 independent three independent experiments.

Acknowledgements
Not applicable.

Author contributions
P.M., F.J.B., and B.v.Z. conceived, designed the project, and wrote the manuscript. P.M., F.J.B., M.S., and S.A. performed experimental work. M.F.T., E.J., and M.C.-P. contributed to experimental design, manuscript review, and editing.

Funding
This work was supported by grants from: BvZ: ANID-FONDECYT (1181645 and 1221745, BvZ), ANID-MILENIO (NCN2023_32, BvZ and FJB), ANID-EXPLORADOR (13220203, BvZ), LifeArc (BvZ), FJB: UNAB DI-06-24/REG, PM: ANID-CONICYT (21151265, PM), SA: ANID-CONICYT (21151265, SA), MCP: National Institutes of Health Grants R01-EY014074 and R01-638 EY014420 (MCP), EJ: ANID-FONDECYT (1151293, EJ), UChile ICBM P2022, EJ.

Availability of data and materials
All data supporting our findings are in the manuscript. Any materials are available upon request.

Declarations

Ethics approval and consent to participate
All experiments conducted in mice were handled according to the guidelines for the handling and care of experimentation established by the NIH (NIH, Maryland, USA) and following the protocol approved by the bioethics committee of Andres Bello University (approval certificate 014/2017).

Consent for publication
Not applicable.

Competing interests
We declare no competing interests.

Received: 26 May 2024 Accepted: 24 September 2024
Published online: 25 October 2024

References

Aguirre T, van Den Bosch L, Goetschalckx K, et al. Increased sensitivity of fibroblasts from amyotrophic lateral sclerosis patients to oxidative stress. Ann Neurol. 1998;43:452–7. https://doi.org/10.1002/ana.410430407.

Al-Chalabi A, Hardiman O. The epidemiology of ALS: a conspiracy of genes, environment and time. Nat Rev Neurol. 2013;9:617–28. https://doi.org/10.1038/nrneurol.2013.203.

Arredondo C, Cefaliello C, Dyrda A, et al. Excessive release of inorganic polyphosphate by ALS/FTD astrocytes causes non-cell-autonomous toxicity to motoneurons. Neuron. 2022;110:1656-1670.e12. https://doi.org/10.1016/j.neuron.2022.02.010.

Aurnhammer C, Haase M, Muether N, et al. Universal real-time PCR for the detection and quantification of adeno-associated virus serotype 2-derived inverted terminal repeat sequences. Hum Gene Ther Part b Methods. 2012;23:18–28. https://doi.org/10.1089/hgtb.2011.034.

Badu-Mensah A, Guo X, McAleer CW, et al. Functional skeletal muscle model derived from SOD1-mutant ALS patient iPSCs recapitulates hallmarks of disease progression. Sci Rep. 2020;10:14302. https://doi.org/10.1038/s41598-020-70510-3.

Barber SC, Shaw PJ. Barber et al-2010-free radical bio med.pdf. Free Radical Bio Med. 2010;48:629–41. https://doi.org/10.1016/j.freeradbiomed.2009.11.018.

Benlefki S, Sanchez-Vicente A, Milla V, et al. Expression of ALS-linked SOD1 mutation in motoneurons or myotubes induces differential effects on neuromuscular function In vitro. Neuroscience. 2020;435:33–43. https://doi.org/10.1016/j.neuroscience.2020.03.044.

Bilan DS, Pase L, Joosen L, et al. Bilan-belousov-HyPer-3- A genetically encoded H2O2 probe with improved performance for ratiometric and fluorescence lifetime imaging-ACS chemical biology_1.pdf. Acs Chem Biol. 2013;8:535–42. https://doi.org/10.1021/cb300625g.

Birger A, Ben-Dor I, Ottolenghi M, et al. Human iPSC-derived astrocytes from ALS patients with mutated C9ORF72 show increased oxidative stress and

neurotoxicity. EBioMedicine. 2019;50:274–89. https://doi.org/10.1016/j.ebiom.2019.11.026.
Bustos FJ, Jury N, Martinez P, et al. NMDA receptor subunit composition controls dendritogenesis of hippocampal neurons through CAMKII, CREB-P, and H3K27ac. J Cell Physiol. 2017;232:3677–92. https://doi.org/10.1002/jcp.25843.
Bustos FJ, Pandian S, Haensgen H, et al. Removal of a partial genomic duplication restores synaptic transmission and behavior in the MyosinVA mutant mouse flailer. BMC Biol. 2023;21:232. https://doi.org/10.1186/s12915-023-01714-y.
Cappello V, Francolini M. Neuromuscular junction dismantling in amyotrophic lateral sclerosis. Int J Mol Sci. 2017;18:2092. https://doi.org/10.3390/ijms18102092.
Chen T-W, Wardill TJ, Sun Y, et al. Ultrasensitive fluorescent proteins for imaging neuronal activity. Nature. 2013;499:295–300. https://doi.org/10.1038/nature12354.
Clement AM, Nguyen MD, Roberts EA, et al. Wild-type nonneuronal cells extend survival of SOD1 mutant motor neurons in ALS mice. Science. 2003;302:113–7. https://doi.org/10.1126/science.1086071.
Cova E, Cereda C, Galli A, et al. Modified expression of Bcl-2 and SOD1 proteins in lymphocytes from sporadic ALS patients. Neurosci Lett. 2006;399:186–90. https://doi.org/10.1016/j.neulet.2006.01.057.
Derave W, Bosch LVD, Lemmens G, et al. Skeletal muscle properties in a transgenic mouse model for amyotrophic lateral sclerosis: effects of creatine treatment. Neurobiol Dis. 2003;13:264–72. https://doi.org/10.1016/s0969-9961(03)00041-x.
Dittlau KS, Bosch LVD. Why should we care about astrocytes in a motor neuron disease? Front Mol Med. 2023;3:1047540. https://doi.org/10.3389/fmmed.2023.1047540.
Dobrowolny G, Giacinti C, Pelosi L, et al. Muscle expression of a local Igf-1 isoform protects motor neurons in an ALS mouse model. J Cell Biol. 2005;168:193–9. https://doi.org/10.1083/jcb.200407021.
Dobrowolny G, Aucello M, Rizzuto E, et al. 4 Dobrowolny, musaro 2008 skeletal muscle is a primary target of SOD1G93A-mediated toxicity.pdf. Cell Metab. 2008;8:425–36. https://doi.org/10.1016/j.cmet.2008.09.002.
Dobrowolny G, Aucello M, Rizzuto E, et al. Skeletal muscle is a primary target of SOD1G93A-mediated toxicity. Cell Metab. 2009;9:110. https://doi.org/10.1016/j.cmet.2008.12.003.
Dupuis L, Oudart H, René F, et al. Evidence for defective energy homeostasis in amyotrophic lateral sclerosis: benefit of a high-energy diet in a transgenic mouse model. Proc Natl Acad Sci. 2004;101:11159–64. https://doi.org/10.1073/pnas.0402026101.
Dupuis L, de Aguilar J-LG, Echaniz-Laguna A, et al. Muscle mitochondrial uncoupling dismantles neuromuscular junction and triggers distal degeneration of motor neurons. PLoS ONE. 2009;4: e5390. https://doi.org/10.1371/journal.pone.0005390.
Etten RAV. Cycling, stressed-out and nervous: cellular functions of c-Abl. Trends Cell Biol. 1999;9:179–86. https://doi.org/10.1016/s0962-8924(99)01549-4.
Fischer LR, Culver DG, Tennant P, et al. Amyotrophic lateral sclerosis is a distal axonopathy: evidence in mice and man. Exp Neurol. 2004;185:232–40. https://doi.org/10.1016/j.expneurol.2003.10.004.
Frey D, Schneider C, Xu L, et al. Early and selective loss of neuromuscular synapse subtypes with low sprouting competence in motoneuron diseases. J Neurosci. 2000;20:2534–42. https://doi.org/10.1523/jneurosci.20-07-02534.2000.
Fritz E, Izaurieta P, Weiss A, et al. Mutant SOD1-expressing astrocytes release toxic factors that trigger motoneuron death by inducing hyperexcitability. J Neurophysiol. 2013;109:2803–14. https://doi.org/10.1152/jn.00500.2012.
Garcés P, Amaro A, Montecino M, van Zundert B. Inorganic polyphosphate: from basic research to diagnostic and therapeutic opportunities in ALS/FTD. Biochem Soc Trans. 2024;52:123–35. https://doi.org/10.1042/bst20230257.
González N, Moresco JJ, Cabezas F, et al. Ck2-Dependent Phosphorylation Is Required to Maintain Pax7 Protein Levels in Proliferating Muscle Progenitors. PLoS ONE. 2016;11: e0154919. https://doi.org/10.1371/journal.pone.0154919.
Guo X, Greene K, Akanda N, et al. In vitro differentiation of functional human skeletal myotubes in a defined system. Biomater Sci. 2013;2:131–8. https://doi.org/10.1039/c3bm60166h.
Guo W, Dittlau KS, Bosch LVD. Axonal transport defects and neurodegeneration: molecular mechanisms and therapeutic implications. Semin Cell Dev Biol. 2020a;99:133–50. https://doi.org/10.1016/j.semcdb.2019.07.010.
Guo X, Badu-Mensah A, Thomas MC, et al. Characterization of functional human skeletal myotubes and neuromuscular junction derived—from the same induced pluripotent stem cell source. Bioengineering. 2020b;7:133. https://doi.org/10.3390/bioengineering7040133.
Gurney ME, Pu H, Chiu AY, et al. Motor neuron degeneration in mice that express a human Cu, Zn superoxide dismutase mutation. Science. 1994;264:1772–5. https://doi.org/10.1126/science.8209258.
Haidet-Phillips AM, Hester ME, Miranda CJ, et al. Astrocytes from familial and sporadic ALS patients are toxic to motor neurons. Nat Biotechnol. 2011;29:824–8. https://doi.org/10.1038/nbt.1957.
Hantschel O, Superti-Furga G. Regulation of the c-Abl and Bcr-Abl tyrosine kinases. Nat Rev Mol Cell Biol. 2004;5:33–44. https://doi.org/10.1038/nrm1280.
Harten ACMV, Phatnani H, Przedborski S. Non-cell-autonomous pathogenic mechanisms in amyotrophic lateral sclerosis. Trends Neurosci. 2021;44:658–68. https://doi.org/10.1016/j.tins.2021.04.008.
Hegedus J, Putman CT, Gordon T. Time course of preferential motor unit loss in the SOD1 G93A mouse model of amyotrophic lateral sclerosis. Neurobiol Dis. 2007;28:154–64. https://doi.org/10.1016/j.nbd.2007.07.003.
Hollenbeck PJ, Saxton WM. The axonal transport of mitochondria. J Cell Sci. 2005;118:5411–9. https://doi.org/10.1242/jcs.02745.
Iguchi Y, Eid L, Parent M, et al. Exosome secretion is a key pathway for clearance of pathological TDP-43. Brain. 2016;139:237. https://doi.org/10.1093/brain/aww237.
Ilieva H, Polymenidou M, Cleveland DW. Ilieva-Non–cell autonomous toxicity in neurodegenerative disorders- ALS and beyond-2009-the journal of cell biology.pdf. J Cell Biol. 2009;187:761–72. https://doi.org/10.1083/jcb.200908164.
Ionescu A, Zahavi EE, Gradus T, et al. Ionescu-Compartmental microfluidic system for studying muscle–neuron communication and neuromuscular junction maintenance-2016-European journal of cell biology.pdf. Eur J Cell Biol. 2016;95:69–88. https://doi.org/10.1016/j.ejcb.2015.11.004.
Jensen L, Jørgensen LH, Bech RD, et al. Skeletal muscle remodelling as a function of disease progression in amyotrophic lateral sclerosis. BioMed Res Int. 2016;2016:5930621. https://doi.org/10.1155/2016/5930621.
Klein A, Maldonado C, Vargas LM, et al. Oxidative stress activates the c-Abl/p73 proapoptotic pathway in Niemann-Pick type C neurons. Neurobiol Dis. 2010;41:209–18. https://doi.org/10.1016/j.nbd.2010.09.008.
Lepore AC, Rauck B, Dejea C, et al. Focal transplantation–based astrocyte replacement is neuroprotective in a model of motor neuron disease. Nat Neurosci. 2008;11:1294–301. https://doi.org/10.1038/nn.2210.
Li Y-C, Zhai X-Y, Ohsato K, et al. Mitochondrial accumulation in the distal part of the initial segment of chicken spinal motoneurons. Brain Res. 2004;1026:235–43. https://doi.org/10.1016/j.brainres.2004.08.016.
Ling S-C, Polymenidou M, Cleveland DW. Converging mechanisms in ALS and FTD: disrupted RNA and protein homeostasis. Neuron. 2013;79:416–38. https://doi.org/10.1016/j.neuron.2013.07.033.
Magrané J, Sahawneh MA, Przedborski S, et al. Mitochondrial dynamics and bioenergetic dysfunction is associated with synaptic alterations in mutant SOD1 motor neurons. J Neurosci. 2012;32:229–42. https://doi.org/10.1523/jneurosci.1233-11.2012.
Maimon R, Perlson E. Muscle secretion of toxic factors, regulated by miR126-5p, facilitates motor neuron degeneration in amyotrophic lateral sclerosis. Neural Regen Res. 2019;14:969–70. https://doi.org/10.4103/1673-5374.250571.
Maimon R, Ionescu A, Bonnie A, et al. miR126-5p downregulation facilitates axon degeneration and NMJ disruption via a non–cell-autonomous mechanism in ALS. J Neurosci. 2018;38:5478–94. https://doi.org/10.1523/jneurosci.3037-17.2018.
Manzano R, Toivonen JM, Calvo AC, et al. Altered in vitro proliferation of mouse SOD1-G93A skeletal muscle satellite cells. Neurodegener Dis. 2013;11:153–64. https://doi.org/10.1159/000338061.
Marchetto MCN, Muotri AR, Mu Y, et al. Non-cell-autonomous effect of human SOD1G37R astrocytes on motor neurons derived from human embryonic stem cells. Cell Stem Cell. 2008;3:649–57. https://doi.org/10.1016/j.stem.2008.10.001.
Martinez A, Lamaizon CM, Valls C, et al. c-Abl phosphorylates MFN2 to regulate mitochondrial morphology in cells under endoplasmic reticulum

and oxidative stress, impacting cell survival and neurodegeneration. Antioxidants. 2023;12:2007. https://doi.org/10.3390/antiox12112007.
Martini M, Dobrowolny G, Aucello M, Musarò A. Postmitotic expression of SOD1G93A gene affects the identity of myogenic cells and inhibits myoblasts differentiation. Mediat Inflamm. 2015;2015: 537853. https://doi.org/10.1155/2015/537853.
Miller KE, Sheetz MP. Axonal mitochondrial transport and potential are correlated. J Cell Sci. 2004;117:2791–804. https://doi.org/10.1242/jcs.01130.
Miller TM, Kim SH, Yamanaka K, et al. Gene transfer demonstrates that muscle is not a primary target for non-cell-autonomous toxicity in familial amyotrophic lateral sclerosis. Proc Natl Acad Sci. 2006;103:19546–51. https://doi.org/10.1073/pnas.0609411103.
Milligan C, Gifondorwa D. Isolation and culture of postnatal spinal motoneurons. Methods Mol Biology Clifton N J. 2011;793:77–85. https://doi.org/10.1007/978-1-61779-328-8_5.
Mishra V, Re DB, Verche VL, et al. Systematic elucidation of neuron-astrocyte interaction in models of amyotrophic lateral sclerosis using multi-modal integrated bioinformatics workflow. Nat Commun. 2020;11:5579. https://doi.org/10.1038/s41467-020-19177-y.
Moloney EB, de Winter F, Verhaagen J. ALS as a distal axonopathy: molecular mechanisms affecting neuromuscular junction stability in the presymptomatic stages of the disease. Front Neurosci. 2014;8:252. https://doi.org/10.3389/fnins.2014.00252.
Nagai M, Re DB, Nagata T, et al. Astrocytes expressing ALS-linked mutated SOD1 release factors selectively toxic to motor neurons. Nat Neurosci. 2007;10:615–22. https://doi.org/10.1038/nn1876.
Papadeas ST, Kraig SE, O'Banion C, et al. Astrocytes carrying the superoxide dismutase 1 (SOD1G93A) mutation induce wild-type motor neuron degeneration in vivo. Proc Natl Acad Sci. 2011;108:17803–8. https://doi.org/10.1073/pnas.1103141108.
Peters OM, Ghasemi M, Brown RH. Emerging mechanisms of molecular pathology in ALS. J Clin Investig. 2015;125:1767–79. https://doi.org/10.1172/jci71601.
Qian K, Huang H, Peterson A, et al. Sporadic ALS astrocytes induce neuronal degeneration In Vivo. Stem Cell Rep. 2017;8:843–55. https://doi.org/10.1016/j.stemcr.2017.03.003.
Renton AE, Chiò A, Traynor BJ. 0 REV renton 2014.pdf. Nat Neurosci. 2014;17:17–23. https://doi.org/10.1038/nn.3584.
Rojas F, Cortes N, Abarzua S, et al. Astrocytes expressing mutant SOD1 and TDP43 trigger motoneuron death that is mediated via sodium channels and nitroxidative stress. Front Cell Neurosci. 2014;8:24. https://doi.org/10.3389/fncel.2014.00024.
Rojas F, Gonzalez D, Cortes N, et al. Reactive oxygen species trigger motoneuron death in non-cell-autonomous models of ALS through activation of c-Abl signaling. Front Cell Neurosci. 2015;9:203. https://doi.org/10.3389/fncel.2015.00203.
Rojas F, Aguilar R, Almeida S, et al. Mature iPSC-derived astrocytes of an ALS/FTD patient carrying the TDP43 A90V mutation display a mild reactive state and release polyP toxic to motoneurons. Front Cell Dev Biol. 2023;11:1226604. https://doi.org/10.3389/fcell.2023.1226604.
Rose T, Jaepel J, Hübener M, Bonhoeffer T. Cell-specific restoration of stimulus preference after monocular deprivation in the visual cortex. Science. 2016;352:1319–22. https://doi.org/10.1126/science.aad3358.
Rosen DR, Siddique T, Patterson D, et al. Mutations in Cu/Zn superoxide dismutase gene are associated with familial amyotrophic lateral sclerosis. Nature. 1993;362:59–62. https://doi.org/10.1038/362059a0.
Saxena S, Caroni P. Selective neuronal vulnerability in neurodegenerative diseases: from stressor thresholds to degeneration. Neuron. 2011;71:35–48. https://doi.org/10.1016/j.neuron.2011.06.031.
Schlatterer SD, Tremblay MA, Acker CM, Davies P. Neuronal c-Abl overexpression leads to neuronal loss and neuroinflammation in the mouse forebrain. J Alzheimer's Dis. 2011;25:119–33. https://doi.org/10.3233/jad-2011-102025.
Sepulveda FJ, Bustos FJ, Inostroza E, et al. Differential roles of NMDA receptor subtypes NR2A and NR2B in dendritic branch development and requirement of rasGRF1. J Neurophysiol. 2010;103:1758–70. https://doi.org/10.1152/jn.00823.2009.
Smolina N, Kostareva A, Bruton J, et al. Primary murine myotubes as a model for investigating muscular dystrophy. BioMed Res Int. 2015;2015: 594751. https://doi.org/10.1155/2015/594751.
Southam KA, King AE, Blizzard CA, et al. Microfluidic primary culture model of the lower motor neuron–neuromuscular junction circuit. J Neurosci Meth. 2013;218:164–9. https://doi.org/10.1016/j.jneumeth.2013.06.002.
Stella R, Bonadio RS, Cagnin S, et al. Secreted metabolome of ALS-related hSOD1(G93A) primary cultures of myocytes and implications for myogenesis. Cells. 2023;12:2751. https://doi.org/10.3390/cells12232751.
Tao H, Gao B. Exosomes for neurodegenerative diseases: diagnosis and targeted therapy. J Neurol. 2024;271:3050–62. https://doi.org/10.1007/s00415-024-12329-w.
Taylor JP, Brown RH, Cleveland DW. Decoding ALS: from genes to mechanism. Nature. 2016;539:197–206. https://doi.org/10.1038/nature20413.
Tong J, Huang C, Bi F, et al. Expression of ALS-linked TDP-43 mutant in astrocytes causes non-cell-autonomous motor neuron death in rats. EMBO J. 2013;32:1917–26. https://doi.org/10.1038/emboj.2013.122.
Torgan CE, Daniels MP. Regulation of myosin heavy chain expression during rat skeletal muscle development in vitro. Mol Biol Cell. 2001;12:1499–508. https://doi.org/10.1091/mbc.12.5.1499.
Towne C, Raoul C, Schneider BL, Aebischer P. Systemic AAV6 delivery mediating RNA interference against SOD1: neuromuscular transduction does not alter disease progression in fALS mice. Mol Ther. 2008;16:1018–25. https://doi.org/10.1038/mt.2008.73.
Tsai KKC, Yuan Z-M. c-Abl stabilizes p73 by a phosphorylation-augmented interaction. Cancer Res. 2003;63:3418–24.
Valdés JA, Hidalgo J, Galaz JL, et al. NF-κB activation by depolarization of skeletal muscle cells depends on ryanodine and IP3 receptor-mediated calcium signals. Am J Physiol-Cell Ph. 2007;292:C1960–70. https://doi.org/10.1152/ajpcell.00320.2006.
van Zundert B, Brown RH. Silencing strategies for therapy of SOD1-mediated ALS. Neurosci Lett. 2017;636:32–9. https://doi.org/10.1016/j.neulet.2016.07.059.
van Zundert B, Izaurieta P, Fritz E, Alvarez FJ. Early pathogenesis in the adult-onset neurodegenerative disease amyotrophic lateral sclerosis. J Cell Biochem. 2012;113:3301–12. https://doi.org/10.1002/jcb.24234.
Vehviläinen P, Koistinaho J, Gundars G. 0 REV Vehvilainen 2014 Mechanisms of mutant SOD1 induced mitochondrial toxicity in amyotrophic lateral sclerosis.pdf. Front Cell Neurosci. 2014;8:126. https://doi.org/10.3389/fncel.2014.00126.
von Maltzahn J, Jones AE, Parks RJ, Rudnicki MA. Pax7 is critical for the normal function of satellite cells in adult skeletal muscle. Proc National Acad Sci. 2013;110:16474–9. https://doi.org/10.1073/pnas.1307680110.
Wang JYJ. Nucleo-cytoplasmic communication in apoptotic response to genotoxic and inflammatory stress. Cell Res. 2005;15:43–8. https://doi.org/10.1038/sj.cr.7290263.
Wang L, Gutmann DH, Roos RP. Astrocyte loss of mutant SOD1 delays ALS disease onset and progression in G85R transgenic mice. Hum Mol Genet. 2011;20:286–93. https://doi.org/10.1093/hmg/ddq463.
Wier CG, Crum AE, Reynolds AB, et al. Muscle contractility dysfunction precedes loss of motor unit connectivity in SOD1(G93A) mice. Muscle Nerve. 2019;59:254–62. https://doi.org/10.1002/mus.26365.
Wong M, Martin LJ. Skeletal muscle-restricted expression of human SOD1 causes motor neuron degeneration in transgenic mice. Hum Mol Genet. 2010;19:2284–302. https://doi.org/10.1093/hmg/ddq106.
Yamanaka K, Chun SJ, Boillee S, et al. Astrocytes as determinants of disease progression in inherited amyotrophic lateral sclerosis. Nat Neurosci. 2008;11:251–3. https://doi.org/10.1038/nn2047.
Yáñez MJ, Belbin O, Estrada LD, et al. c-Abl links APP-BACE1 interaction promoting APP amyloidogenic processing in Niemann-Pick type C disease. Biochim Biophys Acta Mol Basis Dis. 2016;1862:2158–67. https://doi.org/10.1016/j.bbadis.2016.08.016.
Zahavi EE, Ionescu A, Gluska S, et al. 2.1 Perlson, Erez (2015) A compartmentalized microfluidic neuromuscular co-culture system reveals spatial aspects of GDNF functions.pdf. J Cell Sci. 2015;128:1241–52. https://doi.org/10.1242/jcs.167544.

Publisher's Note